A&A 566, A59 (2014)
DOI: 10.1051/0004-6361/201423366

Astronomy & Astrophysics

A simultaneous 3.5 and 1.3 mm polarimetric survey of active galactic nuclei in the northern sky⋆

I. Agudo[1,2,3], C. Thum[4], J. L. Gómez[1], and H. Wiesemeyer[5]

[1] Instituto de Astrofísica de Andalucía (CSIC), Apartado 3004, 18080 Granada, Spain
[2] Institute for Astrophysical Research, Boston University, 725 Commonwealth Avenue, Boston, MA 02215, USA
[3] Current Address: Joint Institute for VLBI in Europe, Postbus 2, 7990 AA Dwingeloo, The Netherlands
e-mail: agudo@jive.nl
[4] Instituto de Radio Astronomía Millimétrica, Avenida Divina Pastora, 7, Local 20, 18012 Granada, Spain
[5] Max-Planck-Institut für Radioastronomie, Auf dem Hügel, 69, 53121 Bonn, Germany

Received 2 January 2014 / Accepted 11 April 2014

ABSTRACT

Context. Short millimeter observations of radio-loud active galactic nuclei (AGN) offer an excellent opportunity to study the physics of their synchrotron-emitting relativistic jets from where the bulk of radio and millimeter emission is radiated. On one hand, AGN jets and their emission cores are significantly less affected by Faraday rotation and depolarization than at longer wavelengths. On the other hand, the millimeter emission of AGN is dominated by the compact innermost regions in the jets, where the jet cannot be seen at longer wavelengths due to synchrotron opacity.
Aims. We present the first simultaneous dual frequency 86 GHz and 229 GHz polarimetric survey of all four Stokes parameters for a large sample of 211 radio-loud active galactic nuclei, designed to be flux limited at 1 Jy at 86 GHz.
Methods. Most of the observations were made in mid-August 2010 using the XPOL polarimeter on the IRAM 30 m millimetric radio telescope.
Results. Linear polarization detections above a 3σ median level of ∼1.0% are reported for 183 sources at 86 GHz and for 23 sources at 229 GHz, where the median 3σ level is ∼6.0%. We show a clear excess of the linear polarization degree that is detected at 229 GHz with regard to that at 86 GHz by a factor of ∼1.6. This implies a progressively better ordered magnetic field for blazar jet regions that are located progressively upstream in the jet. We show that the linear polarization angle at 86 and 229 GHz and the jet structural position angle for both quasars and BL Lacs do not show a clear preference to align in either parallel or perpendicular directions. Our variability study with regard to the 86 GHz data from our previous survey points out a large degree of variation. In particular, we report total flux and linear polarization changes in time scales of years by median factors of ∼1.5 in total flux and ∼1.7 in linear polarization degree (with maximum variations by factors up to 6.3 and ∼5, respectively). Moreover, 86% of sources show linear polarization angles evenly distributed with regard to our previous measurements.

Key words. galaxies: active – galaxies: jets – quasars: general – BL Lacertae objects: general – polarization – surveys

1. Introduction

Among all classes of active galactic nuclei (AGN), radio-loud AGN are characterized by having pairs of relativistic jets of highly energized, magnetized plasma that are ejected along the rotational poles of the super-massive black hole/disk system (e.g., Blandford & Payne 1982). In particular, blazars, the most exotic class of radio-loud AGN, stand out because of the wild variability of their non-thermal jet-emission from radio to γ-rays. Members of this class include BL Lacs and flat spectrum radio quasars (FSRQ, the high power version of the former). The remarkable properties of blazars are affected by strong relativistic effects that beam their radiation and shorten their variability time scales. These properties include superluminal motions (e.g., Gómez et al. 2001; Jorstad et al. 2005; Agudo et al. 2012b), Doppler-boosted emission of the jet pointing at a small angle to the observer (e.g., Kadler et al. 2004), substantial changes in flux and linear polarization, which is sometimes correlated on several spectral ranges on time scales from months (e.g., Bach et al. 2006; Agudo et al. 2011a,b) to hours (e.g., Ackermann et al. 2010; Tavecchio et al. 2010), changes in jet structure (e.g., Jorstad et al. 2007; Agudo et al. 2007), and polarized synchrotron and inverse-Compton emission all along the spectrum (e.g., Marscher et al. 2010; Jorstad et al. 2010; Agudo et al. 2011a,b; Wehrle et al. 2012). The AGN with powerful jets oriented at larger angles to the line of sight (i.e., radio galaxies, the remaining prominent class of radio-loud AGN) suffer less from such relativistic effects; therefore, they display smaller apparent luminosities and longer time scales of variability, although they are thought to be the same astrophysical objects as BL Lacs and FSRQ with the latter being the better oriented counterparts of the former (Urry & Padovani 1995).

Explaining the existence and physical properties of jets from AGN remains one of the greatest current challenges in jet physics. Observations of radio-loud AGN at short millimeter wavelengths offer an excellent opportunity with regard to radio centimeter observations to study these objects for several reasons. First, like AGN radio emission, millimeter emission is well known to be radiated predominantly from the jet with essentially no contribution from the host AGN or its surroundings, which facilitates the interpretation of the measurements in terms of jet physics. Second, AGN jets and, in particular, their millimeter emitting cores are significantly less affected by Faraday rotation and depolarization than at longer wavelengths (see, e.g., Zavala & Taylor 2004; Agudo et al. 2010). Third, the millimeter

⋆ Tables 1 and 2 are available in electronic form at http://www.aanda.org

emission of AGN is dominated by the compact innermost regions in the jets (e.g., Jorstad et al. 2007; Lee et al. 2008), where the jet cannot be seen at longer wavelengths due to synchrotron opacity.

In 2005, we used the XPOL polarimeter (Thum et al. 2008) on the IRAM 30 m telescope to perform the first 3.5 mm (86 GHz) polarization survey of radio-loud AGN over a large (145 source) sample (Agudo et al. 2010). Within the available data, we detected linear polarization above 3σ levels of ∼1.5% for 76% of the sample. Our results pointed out an excess by a factor of ∼2 of 86 GHz linear polarization degree with regard to that at radio wavelengths (15 GHz), suggesting that either the region of bulk millimeter emission has a better ordered magnetic field, or that the radio emission is strongly Faraday depolarized with regard to that at millimeter wavelengths. We also reported a trend of decreasing luminosity toward larger linear polarization degrees within our entire sample, which perhaps indicates a lower magnetic field order for larger luminosity jets. Moreover, in contrast to what was found at radio wavelengths (see Lister & Homan 2005, and references therein), we do not find a relation between the linear polarization angle and the jet structural position angle in either quasars or BL Lacs. Confirmation of this result would imply that no AGN class matches the conditions to show linear polarization angles either parallel or perpendicular to the jet. This should mean that they are intrinsically non-axisymmetric.

Aiming to improve the statistical confidence with regard to previous studies, we performed a new simultaneous 3.5 (86 GHz) and 1.3 mm (229 GHz) AGN polarimetric survey with the XPOL polarimeter on the IRAM 30 m telescope in polarimetric mode over an updated and increased sample of 211 sources that was designed to be 1 Jy total-flux limited. Our new observations were also contemporaneous with current large surveys at other spectral ranges, therefore allowing for multi-spectral range studies. The dual frequency configuration of our observing program also allowed us to search for large Faraday rotation effects in bright AGN, whereas the comparison with our previous survey allowed us to study the total flux and polarization AGN variability at short millimeter wavelengths in bright AGN. In this paper, we describe this new survey and the results from the analysis of the resulting data. The comparison of the data from this new survey with γ-ray measurements from the Fermi-LAT 2-year AGN Catalog (Ackermann et al. 2011) and a detailed statistical study of their correlation are presented in a separate paper (Agudo et al., in prep.).

2. The sample

Table 1 shows the list of 211 sources covered by our new survey and some of the most prominent properties of every source. This list comprises the 102 AGN in our previous 3.5 mm AGN Polarization survey that are brighter than 0.9 Jy plus 109 additional AGN sources with and estimated[1] 90 GHz flux density $S_{90\ \mathrm{GHz}} > 0.9$ Jy contained in the WMAP (*Wilkinson* Microwave Anisotropy Probe) 7-Year Catalog of Point Sources (Gold et al. 2011) with declination $>-30°$ in J2000.0. Below this declination limit, no source can be observed at $\gtrsim 20°$ elevation from the IRAM 30 m telescope.

Hence, our source list was designed to build a 3.5 mm 1 Jy flux-limited complete sample of AGN. However, our observations have revealed that 108 of the 211 observed sources showed $S_{86} < 1$ Jy and even 47 had $S_{86} < 0.5$ Jy. We attribute this result to both total-flux source variability, which reached a factor of 1.5 for 50% of sources in our sample (see Sect. 6), and inaccuracies in the estimated $S_{90\ \mathrm{GHz}}$ fluxes from the WMAP 7-Year Catalog for candidate sources. Indeed, ∼40 sources of the WMAP 7-year sample do not match our selection criteria, while they do so in the 9-year WMAP sample, which is assumed to include more precise measurements of the weaker objects.

Radio-loud AGN with relatively large luminosities at millimeter wavelengths are dominated by relativistically enhanced flat spectrum radio emission from the innermost jet regions in AGN, whereas the emission from steep spectrum radio sources, typically weak or undetectable at millimeter wavelengths, comes from giant radio lobes of radio galaxies. Because of the spectral criteria applied to select the sources in our previous 3.5 mm survey, this sample was dominated by flat spectrum radio sources (i.e., FSRQ and BL Lacs). Therefore, our sample is dominated by blazars. In particular, our new 3.5 and 1.3 mm AGN Polarization Survey sample contains 152 quasars, 32 BL Lacs, and 21 radio galaxies with six unclassified sources, i.e., not contained in the Véron-Cetty & Véron (2006) catalog. Thus, our new 3.5 and 1.3 mm AGN Polarization Survey sample is adequate for studies of the mm-polarimetric properties of quasar and BL Lac blazars.

Moreover, 110 of our sources are contained in the MOJAVE 15 GHz VLBI Survey of bright AGN jets (Lister et al. 2009), and 83% of MOJAVE sources are in our sample. This high rate of coincidence shows that the two samples are adequate for comparative studies.

The source redshift in the entire sample ranges from $z = 0.00068$ to $z = 3.408$ with a mean and median at $\bar{z} = 0.937$ and $\tilde{z} = 0.859$, respectively.

3. Observations and data reduction

The observations were performed with the XPOL polarimeter (Thum et al. 2008) connected to the E090 and E230 EMIR receiver system (Carter et al. 2012) on the IRAM 30 m telescope. The advanced design of EMIR allowed us to perform the observations simultaneously at 3.5 mm (86 GHz with the E090 pair of orthogonal receivers) and 1.3 mm (229 GHz with the E230 pair of orthogonal receivers) without loss of a significant amount of signal at either waveband (Thum et al. 2008). The flexibility of the VESPA autocorrelator in polarimetric mode (i.e., XPOL) also allows us to simultaneously process the 86 and 229 GHz signals, although with a limited bandwidth of 640 MHz for each of the two orthogonally polarized receivers of the E090 band and 320 MHz for those of the E230 band.

The bulk of the observing program was performed from 13 to 16 August 2010, although a small number of remaining observations were done several weeks before (from May 5, 2010) or after (until June 16, 2011) to complete observations of missing sources or initially unreliable measurements; see Table 2.

To perform the observations, we employed the standard XPOL set-up and calibration method discussed in Thum et al. (2008). Our observing strategy was essentially the same as the one used for our previous 3.5 mm AGN Polarimetric Survey (Agudo et al. 2010). We made a continuous refinement of the pointing model of the telescope before every polarization integration, as well as frequent measurements of the focus parameters and polarization calibrators (Mars and Uranus).

[1] Note that the $S_{90\ \mathrm{GHz}}$ WMAP fluxes were estimated from extrapolation from the WMAP spectra and spectrum $S_{60\ \mathrm{GHz}}$ where a $S_{90\ \mathrm{GHz}}$ was not available.

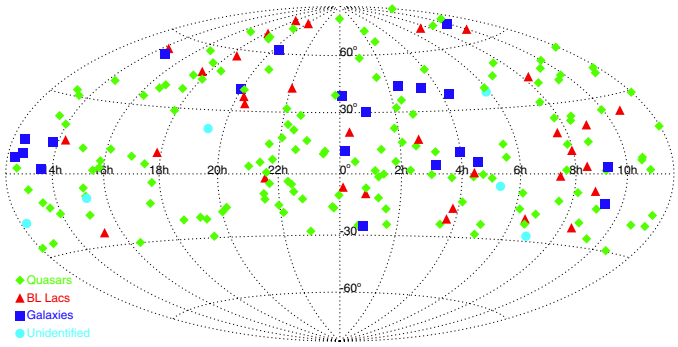

Fig. 1. Sky distribution of sources in our sample in J2000.0 coordinates.

For the data reduction, we followed the procedure in Agudo et al. (2010). The instrumental polarization removed from the data was the one estimated from observations of unpolarized calibrators, which is $Q_{i,86} = -0.7 \pm 0.3\%$, $U_{i,86} = -0.3 \pm 0.2\%$ and $V_{i,86} = 0.0 \pm 0.3\%$ for 86 GHz observations, and $Q_{i,229} = -0.4 \pm 1.5\%$, $U_{i,229} = -1.1 \pm 1.5\%$, and $V_{i,229} = 2.4 \pm 0.6\%$ for 229 GHz. These instrumental polarization parameters are fully consistent with those measured during the first months of operation of EMIR connected to XPOL. After applying all polarization calibrations, we obtained final polarization-error medians of $\Delta\tilde{m}_{\rm L}^{86} \approx 0.32\%$, $\Delta\tilde{\chi}^{86} \approx 3°$, and $\Delta\tilde{m}_{\rm C}^{86} \approx 0.35\%$ for the linear polarization degree ($m_{\rm L}$), the linear polarization electric vector position angle (χ), and the circular polarization degree ($m_{\rm C}$) at 86 GHz, respectively. For the observations at 229 GHz, we obtained $\Delta\tilde{m}_{\rm L}^{229} \approx 2\%$, $\Delta\tilde{\chi}^{229} \approx 7°$, and $\Delta\tilde{m}_{\rm C}^{229} \approx 2\%$. For the conversion from antenna temperatures to flux densities, we used standard calibration factors of $C_{\rm Jy/K^{86}} = 6.4$ Jy/K and $C_{\rm Jy/K^{229}} = 9.3$ Jy/K at 86 and 229 GHz, respectively (e.g., Agudo et al. 2006).

4. Results

Table 2 shows the results of the new 86 and 229 GHz observations presented here. With the source name, we give the integration time, the total flux density (S_{86} and S_{229} at 86 and 229 GHz, respectively), the fractional linear polarization ($m_{\rm L,86}$ and $m_{\rm L,229}$), the linear polarization angle (χ_{86} and χ_{229}), the fractional circular polarization at 86 GHz ($m_{\rm C,86}$), and the maximum Faraday rotation allowed from the χ_{86} and χ_{229} measurements. For both 86 and 229 GHz observations, 3σ upper limits in S, $m_{\rm L}$, and/or $m_{\rm C}$ were provided whenever the measurement did not exceed its corresponding 3σ value. In Fig. 1, we also show the sky distribution of sources in our sample.

Whereas 86 GHz linear polarization was detected from most sources in our sample (88%), 86 GHz circular polarization was detected for a small fraction of them only (6%). At 229 GHz, the lower flux density values of most sources in our sample, the reduced sensitivity and the poorer sky transmission at this waveband only allowed us to detect linear polarization from 13% of our sample. No circular polarization was detected at 229 GHz.

In the following subsections, we present the statistical analysis and discussion of the relevant aspects regarding these data.

4.1. Total flux density

4.1.1. Total luminosity

Figures 2 and 3 show the 86 and 229 GHz luminosity ($L = 4\pi d_{\rm L}^2 S(1+z)^{-1}$, where $d_{\rm L}$ is the luminosity distance[2]) as a function of redshift in our sample. A significant fraction of sources (51% [22%]) show 86 GHz flux densities below the 1 Jy (0.5 Jy) threshold, whereas only a small subset of eight sources (4%) shows $S_{86} > 5$ Jy. At 229 GHz, 80% (48%) of the sources show flux densities below 1 Jy (0.5 Jy), and only 6 of them (3%) are brighter than 5 Jy. As expected, cosmologically distant quasars show the largest luminosities with a median $\tilde{L}_Q^{86} = 2.7\times10^{27}$ W/Hz ($\tilde{L}_Q^{229} = 1.6\times10^{27}$ W/Hz), followed by BL Lac objects with $\tilde{L}_B^{86} = 3.8\times10^{26}$ W/Hz ($\tilde{L}_B^{229} = 1.9\times10^{26}$ W/Hz), and radio galaxies $\tilde{L}_G^{86} = 8.0\times10^{24}$ W/Hz ($\tilde{L}_G^{229} = 6.8\times10^{24}$ W/Hz). This is consistent with expectations from the AGN unification theory (Urry & Padovani 1995), where quasars and BL Lacs are the relativistically Doppler boosted (i.e., beamed) versions of high power and low power radio galaxies (with their jets oriented closer to the plane of the sky), respectively.

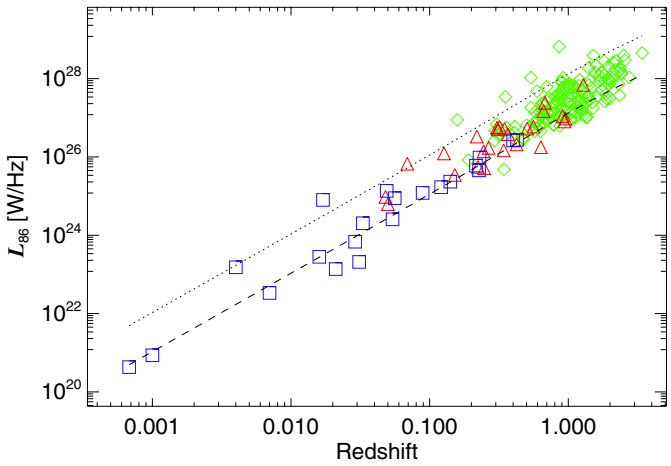

Fig. 2. 86 GHz luminosity as a function of redshift. The dashed line indicates the luminosity for the observer's frame flux density $S_{86} = 0.5$ Jy, whereas the dotted line is for $S_{86} = 5$ Jy. As for other figures hereafter, diamonds symbolize quasars, triangles denote BL Lacs, and squares are radio galaxies.

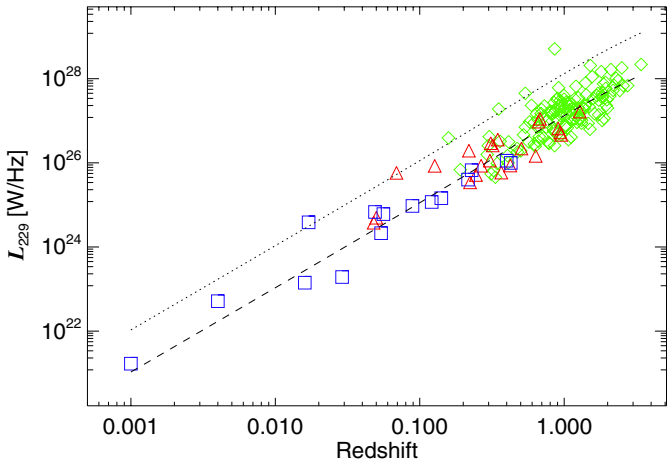

Fig. 3. 229 GHz luminosity as a function of redshift. The dashed line indicates the luminosity for observer frame's flux density $S_{229} = 0.5$ Jy, whereas the dotted line is for $S_{229} = 5$ Jy.

4.1.2. Spectral index

To study the spectral differences between quasars and BL Lacs, we determined the 15 to 86 GHz spectral index[3] ($\alpha_{15,86}$) of

[2] We use hereafter a $H_{\rm o} = 71\,{\rm km\,s^{-1}\,Mpc^{-1}}$, $\Omega_{\rm m} = 0.27$, and $\Omega_\Lambda = 0.73$ cosmology.

[3] We define the spectral index between two observing frequencies ν_1 and ν_2 as $\alpha_{\nu_1,\nu_2} = \log(S_{\nu_1}/S_{\nu_2})/\log(\nu_1/\nu_2)$.

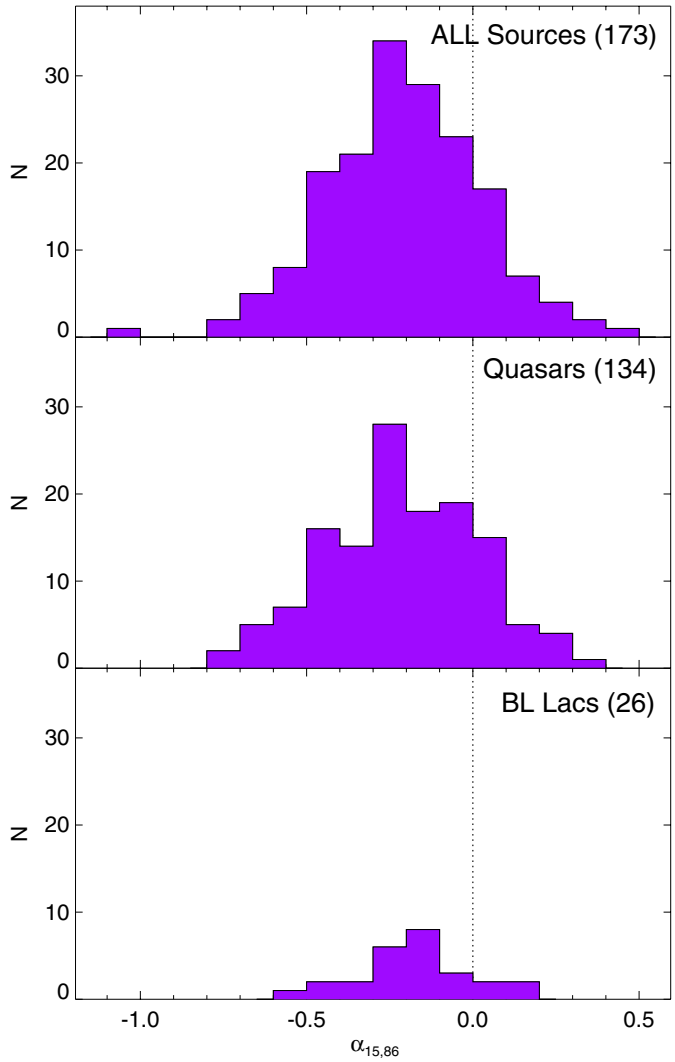

Fig. 4. Distribution of 15 GHz to 86 GHz spectral indices ($\alpha_{15,86}$) for all sources in both the MOJAVE and our sample, and their corresponding quasar and BL Lac sub-samples. The 15 GHz total flux density was taken from integrated intensity of MOJAVE images. For each source, the 15 GHz observation taken at the closest date to our 86 GHz measurement was selected. Numbers in parentheses denote sample sizes.

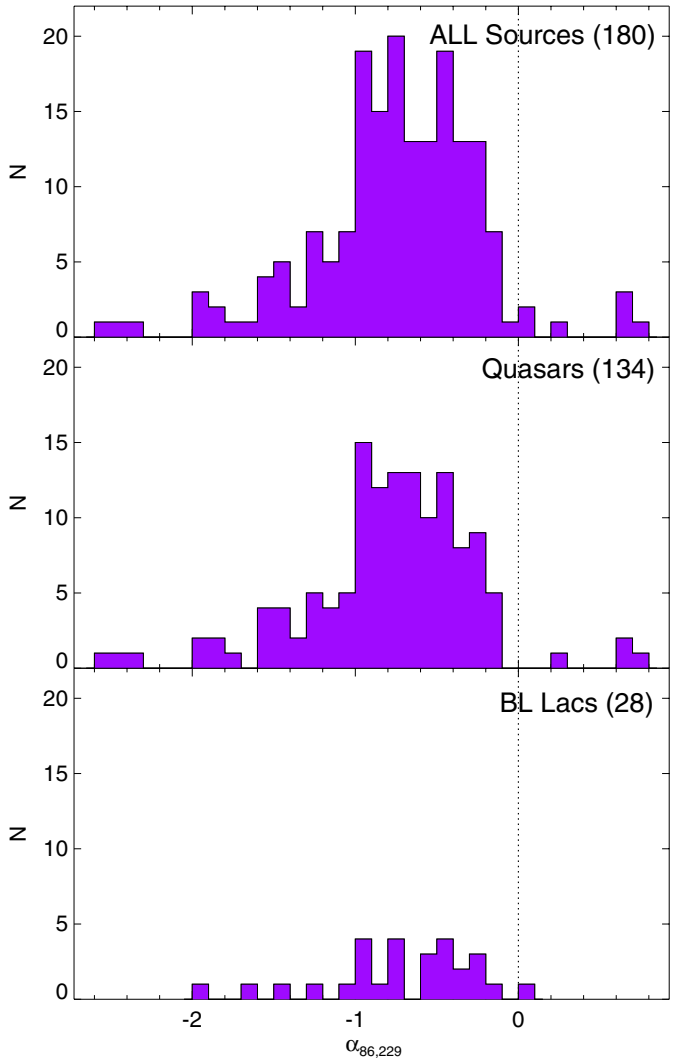

Fig. 5. Distribution of 86 GHz to 229 GHz spectral indices ($\alpha_{86,229}$) for all sources detected at both frequencies in our sample.

quasars and BL Lacs. For that, we used the 15 GHz total flux densities from integrated intensities in available MOJAVE VLBA images[4] with observations performed as contemporaneous as possible to our millimeter observations.

Similar to what it was found in Agudo et al. (2010), Fig. 4 shows that the $\alpha_{15,86}$ spectral indices for both quasars and BL Lacs are distributed toward flat and optically thin spectral indices (with $\alpha_{15,86}$ median $\tilde{\alpha}^{\rm Q}_{15,86} = -0.22$ for quasars and $\tilde{\alpha}^{\rm B}_{15,86} = -0.12$ for BL Lacs). Only a small fraction of sources (19% of quasars and 15% of BL Lacs) show $\alpha_{15,86} > 0$. The smallest average spectral index of quasars with regard to that of BL Lacs is consistent with the well-known trend for BL Lacs to distribute the peaks of their synchrotron spectral energy distributions toward higher frequencies than quasars (e.g., Ackermann et al. 2011; Giommi et al. 2013). We also attribute part of the differences in spectral index between quasars and BL Lacs to the larger cosmological redshifts of quasars that shifts their spectra to lower frequencies in the observer's frame.

[4] http://www.physics.purdue.edu/MOJAVE

The 86 to 229 spectral index distribution ($\alpha_{86,229}$, see Fig. 5) also shows a similar trend with BL Lacs distributed toward slightly smaller spectral indexes with regard to quasars, although both the quasar and the BL Lac samples are distributed toward significantly smaller (more optically thin) spectral indexes (with $\tilde{\alpha}^{\rm Q}_{86,229} = -0.75$ for quasars and $\tilde{\alpha}^{\rm B}_{86,229} = -0.56$ for BL Lacs) for the case of $\alpha_{86,229}$. These values are consistent with those for optically thin synchrotron radiation from AGN jets (Rybicki & Lightman 1979), which shows that blazars display optically thin radiation between 86 and 229 GHz in general and also guarantees that our polarimetric observations were not significantly affected by polarization angle rotation and depolarization owing to opacity effects. There are, however, a few exceptions, in particular 21 out of 180, for which the spectral index is flat or optically thick (with $\alpha_{86,229} \gtrsim 0.25$), perhaps, because of ongoing prominent flaring states (e.g., Marscher & Gear 1985).

4.2. Linear polarization

Fractional linear polarization at 86 GHz ($m_{\rm L,86}$) was detected at $\geq 3\sigma$ level for 183 sources; this is 88% of the entire sample detected in total flux at 86 GHz (Fig. 6). At 229 GHz, the reduced sensitivity of our observations only allowed us to

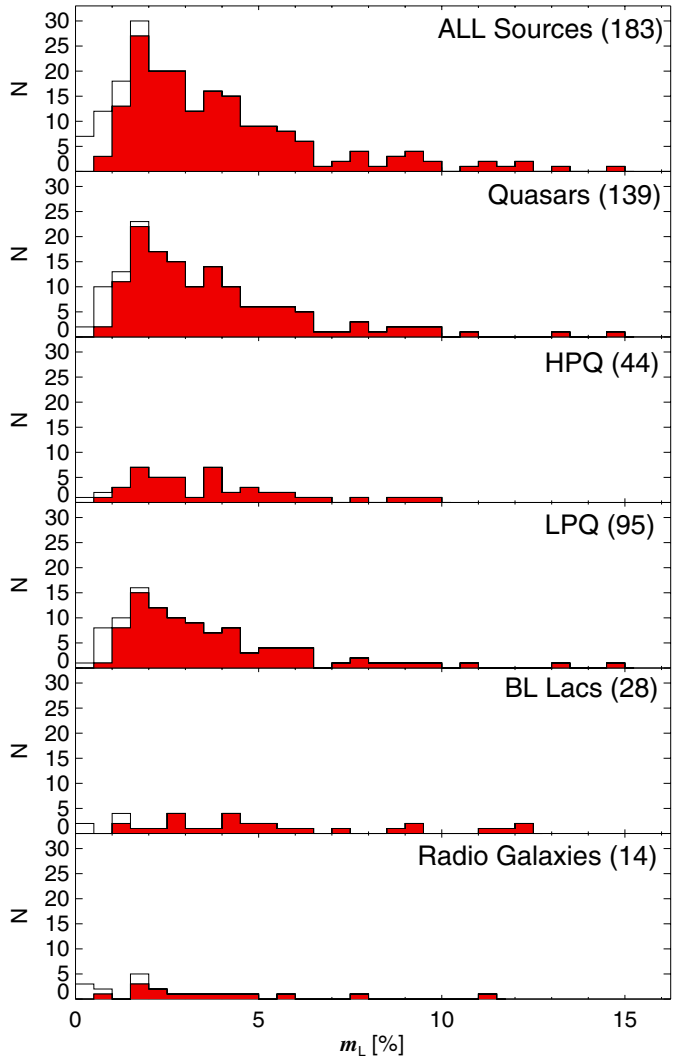

Fig. 6. Distribution of 86 GHz fractional linear polarization (red areas) for all sources in the sample, quasars, high optical polarization quasars (HPQ), low optical polarization quasars (LPQ), BL Lacs, and radio galaxies *from top to bottom*. *N* is the number of sources in 0.5% wide bins. Non-filled areas also include non-detection upper limits. Since we chose 3σ upper limits with a mean $\bar{\sigma}_{m_{\rm L,86}} \approx 0.32\%$, there are only a few detections at $m_{\rm L,86} \lesssim 0.96\%$.

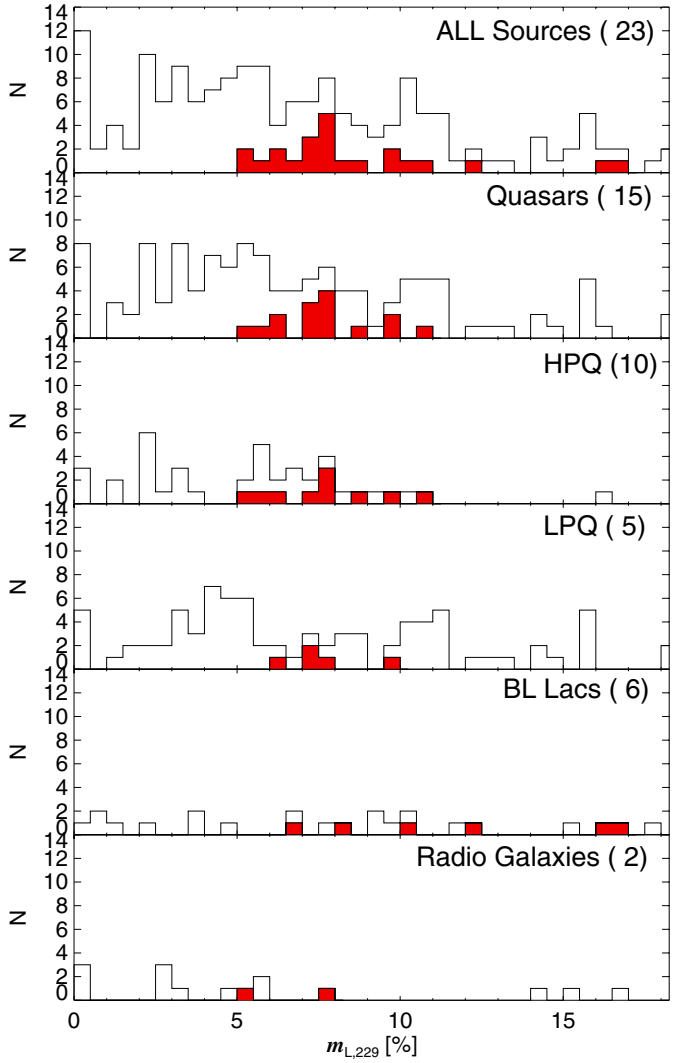

Fig. 7. Same as Fig. 6 but for 229 GHz fractional linear polarization. Since we chose 3σ upper limits with mean $\bar{\sigma}_{m_{\rm L,229}} \approx 2.0\%$, there are only a few detections at $m_{\rm L,229} \lesssim 6.0\%$.

detect 23 sources. This corresponds to a 13% of all 181 sources detected at 229 GHz in total flux (Fig. 7).

We find the median values of $m_{\rm L,86}$ for BL Lacs ($\tilde{m}^{\rm B}_{\rm L,86} = 4.6\%$) to be appreciably larger than those for quasars ($\tilde{m}^{\rm Q}_{\rm L,86} = 3.2\%$). A similar result is found for the 229 GHz linear polarization degree, where ($\tilde{m}^{\rm B}_{\rm L,229} = 12.0\%$) is also much larger than for quasars ($\tilde{m}^{\rm Q}_{\rm L,86} = 7.7\%$). To make these comparisons, 3σ upper limits of values of $m_{\rm L}$ were considered for non-detections of linear polarization to avoid overestimating the median of $m_{\rm L}$. The difference in the BL Lac and the quasar distributions of the linear polarization degree is confirmed by Gehan's generalized Wilcoxon (GGW) test[5] at 97.1% confidence level[6] for the 86 distributions. Although the same test at 229 GHz gives a 99.9% confidence that the BL Lac and quasar distributions are different, this result should be taken with care given the low number statistics at this frequency. This result (i.e., quasars significantly less polarized than BL Lacs at millimeter wavelengths) was already pointed out at 86 GHz in Agudo et al. (2010).

The differences in the linear polarization degree of quasars and BL Lacs cannot be explained by differences in opacity in these two classes of sources, since we have already shown that both of them are in general optically thin between 86 and 229 GHz for most sources in their corresponding samples. Hovatta et al. (2009) and Pushkarev et al. (2009) suggested that quasars have, in general, smaller viewing angles than BL Lacs. The lower polarization degree of quasars with regard of BL Lacs that we report agree with these two studies. If quasars have smaller viewing angles than BL Lacs, the former should be affected by stronger depolarization along the line of sight. This requires the assumption that the magnetic fields in the jets of both quasars and BL Lacs are not homogeneously distributed along the jet axis or that their jets themselves are not axisymmetric.

[5] The Gehan's generalized Wilcoxon test (Gehan 1965) considers both detections and upper limits. To perform our tests, we used the ASURV 1.2 survival analysis package (see Lavalley et al. 1992, and references therein).

[6] Throughout this paper, only confidence levels ≥95.0% will be considered sufficiently high to claim that two distributions are significantly different.

In Agudo et al. (2010), we pointed out an apparent dichotomy in the 86 GHz distribution of the linear polarization degree of our entire source sample, which showed a peak at $m_{\mathrm{L},86} \approx 2.5\%$ and a second one at $m_{\mathrm{L},86} \approx 4\%$. This behavior was also found at lower polarization degrees by Lister & Homan (2005) for the cores of quasars and the integrated polarization degree of EGRET-detected blazars. The data from our new survey further confirms the dichotomy found in Agudo et al. (2010). The $m_{\mathrm{L},86}$ distribution of the entire source sample (top panel of Fig. 6) also shows a hint of this dichotomy with the first peak in the range $m_{\mathrm{L},86} \in [1.5, 2.5]\%$, and the second one at $m_{\mathrm{L},86} \approx 4\%$. The lack of enough polarization sensitivity of our 229 GHz observations with regard to those at 86 GHz prevents us from studying this dichotomy at 229 GHz, where linear polarization below the 5% level is not detected (Fig. 7).

The similarity of the 86 GHz $m_{\mathrm{L},86}$ distributions of the entire source sample and that of quasars (that, however, only has a confidence of 78.9% according to our GGW test) might indicate that this dichotomy is produced by quasars but not by BL Lacs. Indeed, the $m_{\mathrm{L},86}$ distribution of BL Lacs is significantly different than those of quasars, see above. Here, we test the hypothesis that the bimodal $m_{\mathrm{L},86}$ is produced by high optical polarization quasars (HPQ, for the high polarization peak in the $m_{\mathrm{L},86}$ distribution of quasars) as listed in Véron-Cetty & Véron (2006) and low optical polarization quasars (LPQ, for the low polarization peak). This, however, does not seem to be a reliable explanation, given that the HPQ $m_{\mathrm{L},86}$ distribution is not clearly accumulated toward large linear polarization degrees, and we do not have the means to statistically demonstrate that the HPQ and LPQ m_{L} distributions are significantly different (the GGW test gives only a 52.6% confidence for that). Therefore, although we have been able to confirm the dichotomy in the $m_{\mathrm{L},86}$ distribution of our entire source sample (quasars in particular), our new data remain inconclusive about the possible physical meaning of this apparent dichotomy.

4.2.1. Fractional linear polarization ratio along the radio and millimeter spectrum

The linear polarization detection rate in our survey is ∼88% at 86 GHz and ∼13% at 229 GHz (see above). The 3σ level of linear polarization detection has medians of $3\tilde{\sigma}_{m_{\mathrm{L},86}} \sim 1.0\%$ at 86 GHz and $3\tilde{\sigma}_{m_{\mathrm{L},229}} \sim 6.0\%$ at 229 GHz. Therefore, ∼88% of our sources detected in total flux at 86 GHz show $m_{\mathrm{L},86} \gtrsim 1.0\%$, and ∼13% of those detected in total flux at 229 GHz show $m_{\mathrm{L},229} \gtrsim 6.0\%$.

In contrast, 71% of the sources in both the MOJAVE and in our sample of 86 GHz detections show $m_{\mathrm{L},86} \gtrsim 1.0\%$, whereas only 8% of MOJAVE sources with linear polarization detected at 229 GHz display $m_{\mathrm{L},229} \gtrsim 6.0\%$. This points out a progressive increasing dependence of the fractional linear polarization of blazars with observing frequency (see also Agudo et al. 2006, 2010; Jorstad et al. 2007). This can also be discerned from Figs. 6 and 7.

By using the data from our first 3.5 AGN Polarimetric Survey in Agudo et al. (2010), we demonstrated that the 86 GHz linear polarization degree of blazars was, in general, around twice that at 15 GHz. Figure 8, where we plot the distributions of $m_{\mathrm{L},86}/m_{\mathrm{L},15}$ for those sources detected at 86 GHz in our survey and also with available contemporaneous 15 GHz MOJAVE measurements of the linear polarization degree, also show the same result. The entire source sample, quasars, and BL Lacs show significantly larger fractional linear polarization at 86 GHz than at 15 GHz by a mean factor ≈2 (Fig. 8). Essentially, the same result is found for the distributions of $m_{\mathrm{L},229}/m_{\mathrm{L},86}$, when the linear polarization of sources detected at 229 GHz in our survey is compared with their corresponding, simultaneously measured, 86 GHz linear polarization degree (Fig. 9). The median values of the $m_{\mathrm{L},86}/m_{\mathrm{L},15}$ and $m_{\mathrm{L},229}/m_{\mathrm{L},86}$ distributions show, however, slightly smaller values: 1.6, 1.6, and 1.5 for the entire sample, quasars, and BL Lacs, respectively, for the case of $m_{\mathrm{L},86}/m_{\mathrm{L},15}$ and 1.7, 1.7, and 1.5 for $m_{\mathrm{L},229}/m_{\mathrm{L},86}$.

Although there are some apparent differences in the different distributions shown in Figs. 8 and 9, our Kolmogorov–Smirnov (K-S) tests do not give a sufficiently high confidence to conclude that the quasar and BL Lac distributions of $m_{\mathrm{L},86}/m_{\mathrm{L},15}$ and $m_{\mathrm{L},229}/m_{\mathrm{L},86}$ are selected from different parent distributions (confidence level only 40.9%, and 88.3%, respectively). Note that there is also a prominent 18% (9%) fraction of sources with $m_{\mathrm{L},86}/m_{\mathrm{L},15}$ ($m_{\mathrm{L},229}/m_{\mathrm{L},86}$) ratio greater than 4. Such a tail of large, high-frequency linear-polarization excess seems to be present in both quasars and BL Lacs, although BL Lacs do not

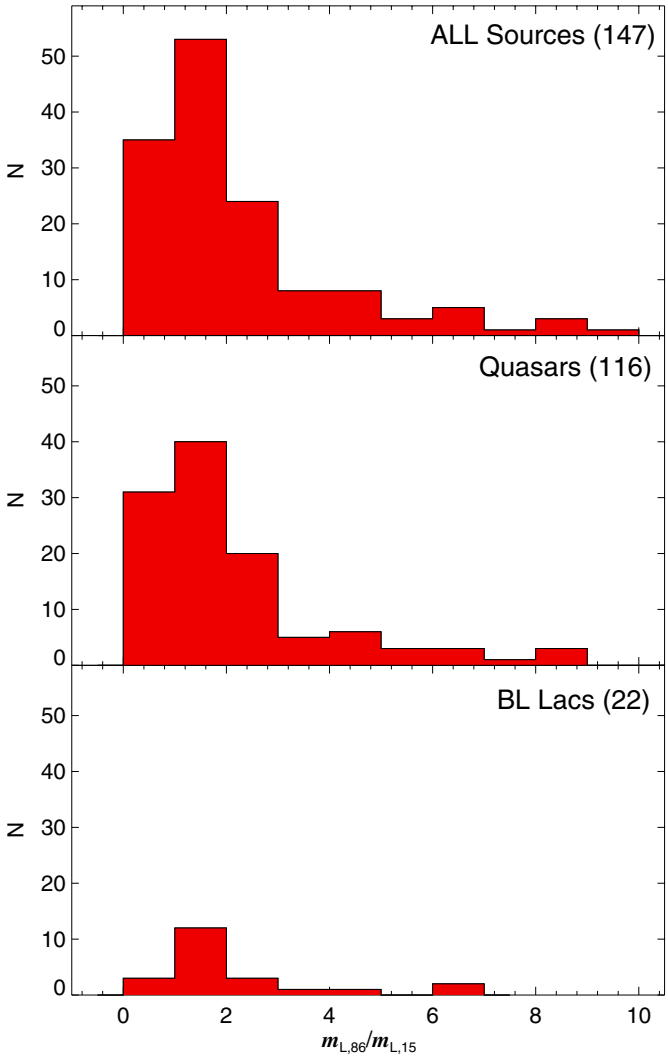

Fig. 8. Distribution of 86 GHz to 15 GHz fractional linear polarization ratio for sources with detected linear polarization in both our survey and MOJAVE. Six sources in the range $10 < m_{\mathrm{L},86}/m_{\mathrm{L},15} < 19$ are not shown. The 15 GHz linear polarization fraction was computed from measurements of integrated total flux density and linearly polarized flux density from 15 GHz VLBI images taken by the MOJAVE team on the closest available dates to our 86 GHz observations.

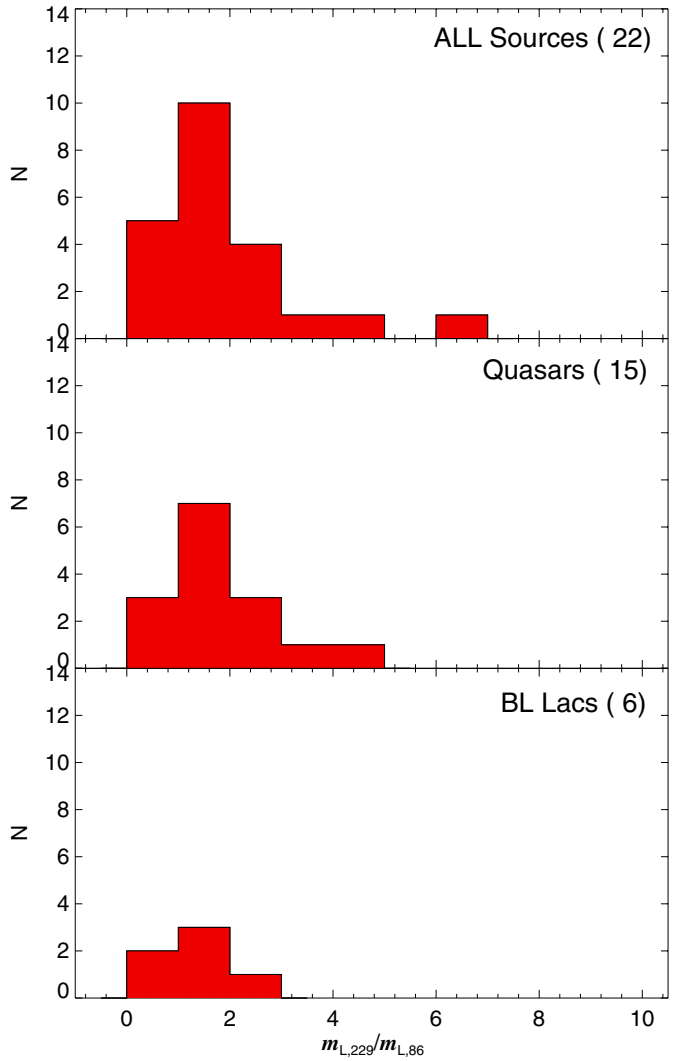

Fig. 9. Distribution of 229 GHz to 86 GHz fractional linear polarization ratio for sources with detected linear polarization at both frequencies (i.e., $m_{L,229}/m_{L,86}$).

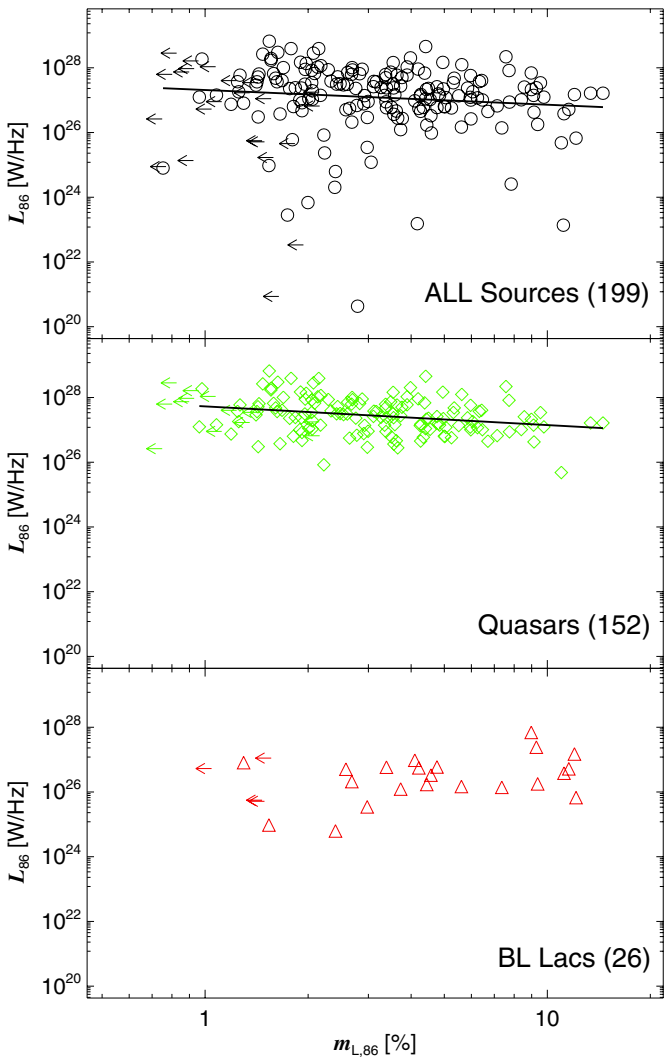

Fig. 10. 86 GHz luminosity versus fractional linear polarization at 86 GHz for sources with known redshift for the entire source sample, quasars, and BL Lacs (from *top to bottom*). Arrows symbolize m_L upper limits. The continuous lines symbolize the result of linear regressions. Numbers in parentheses denote sample sizes.

show it so clearly in $m_{L,229}/m_{L,86}$, perhaps, because of the lower number of sources in that sub-sample.

To explain the observed excess of $m_{L,86}$ with regard to $m_{L,15}$ by a factor of 2 (Agudo et al. 2010), we proposed two complementary explanations for this effect: a) that the 86 GHz emission in blazars comes from a region with a better ordered magnetic field than the 15 GHz one; and b) that the 15 GHz emission from blazars is affected by a considerably greater Faraday depolarization relative to the 86 GHz emission. Now that we have also studied the properties of the $m_{L,229}/m_{L,86}$ distributions in this work, we can safely assume that explanation b) is not reliable, at least for the comparison of the 86 and the 229 GHz emission, which is very unlikely to show appreciable Faraday rotations for a significant number of sources in our samples (see Sects. 1 and 4.3). Option a), along with the existing evidence that higher millimeter emission from blazars comes from inner regions upstream in their jets (e.g., Jorstad et al. 2007), imply that the magnetic field is progressively better ordered in blazar jet regions that are located progressively upstream in the jet.

4.2.2. Total luminosity vs. linear polarization

In Agudo et al. (2010), we reported a significant anti-correlation for the first time between the 86 GHz luminosity (L_{86}) and the $m_{L,86}$ distribution for blazars in our previous 3.5 mm AGN Polarization Survey. The data from our new survey also reproduces such anti-correlation. Figure 10 shows L_{86} versus $m_{L,86}$ for sources with a known redshift in the entire source sample, quasars, and BL Lacs. Our Spearman's ρ test for correlation gives $\rho = -0.22$ with a 99.7% confidence for the entire source sample and $\rho = -0.27$ with 99.9% confidence for quasars. Possibly because of the soft dependence of L_{86} versus $m_{L,86}$ and also because of the small number of measurements for BL Lacs, this anti–correlation cannot be confirmed for BL Lacs, for which $\rho = 0.25$ with 74.5% confidence. A similar analysis performed through the Generalized Spearman's ρ test, made by using the ASURV 1.2 package by Lavalley et al. (1992), that takes into account both detections and upper limits, also points out statistically significant anti-correlation for quasars with $\rho = -0.27$ at 99.9% confidence. The Generalized Spearman's ρ test only gives 91.2% confidence for $\rho = -0.12$ for the entire source sample when upper limits are accounted for, and even less ($\rho = 0.24$ at 76.9% confidence) for BL Lacs. At 229 GHz, the small number of linear polarization detections do not allow for reliable correlation studies of L_{229} versus $m_{L,229}$.

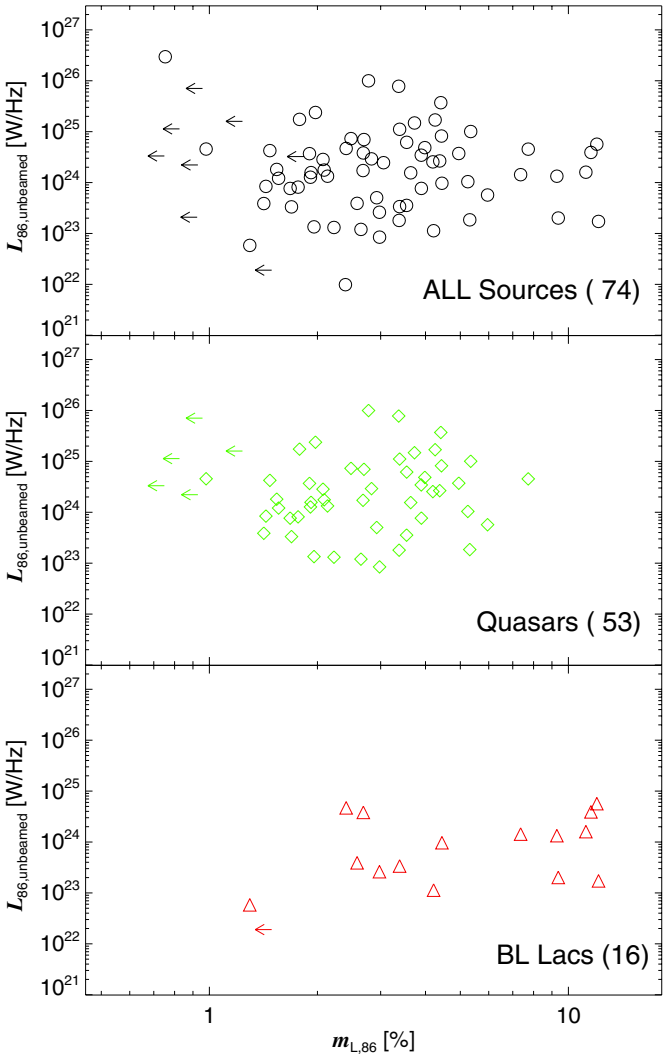

Fig. 11. Same as Fig. 10 but for unbeamed 86 GHz luminosities computed from Doppler factors given in Hovatta et al. (2009).

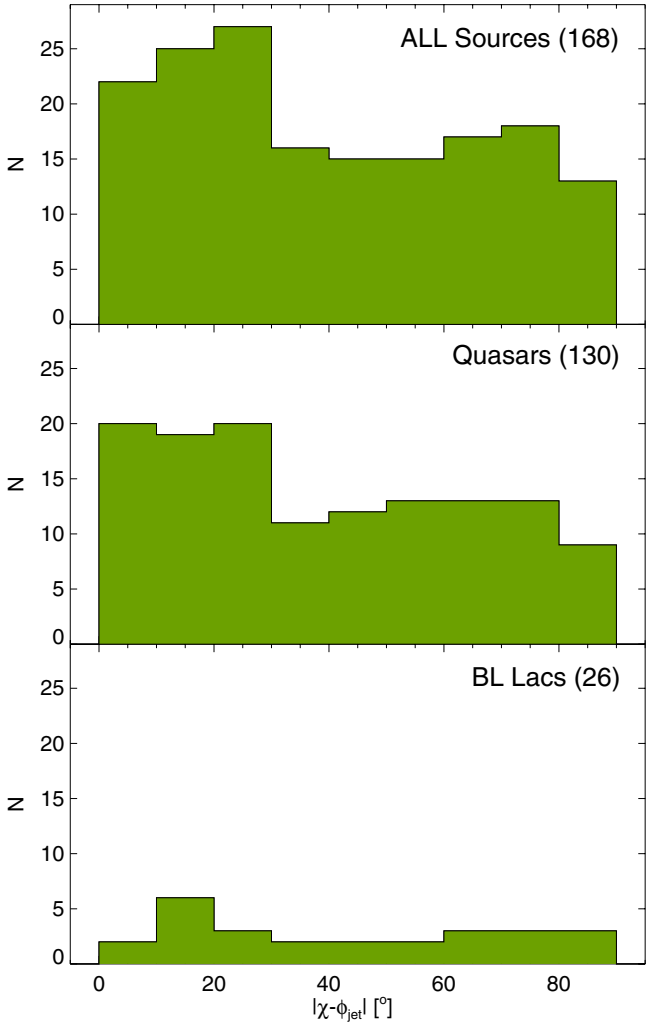

Fig. 12. Distribution of misalignment between χ_{86} and ϕ_{jet}. *From top to bottom*, we present, the entire source sample, the quasar, and the BL Lac sub-samples.

The confirmation of this result implies that the magnetic field order in jets of blazars increases with decreasing millimeter luminosity. In Agudo et al. (2010), we tested the hypothesis that the L versus m_{L} anti-correlation would be only produced by orientation and relativistic effects; that is, the sources whose jets are better oriented to the line of sight are expected to display larger luminosities (because of their larger Doppler boosting) and also lower linear polarization degrees (because of cancellation of orthogonal polarization components along the line of sight). This was tested by computing the unbeamed luminosities ($L_{86,\,\mathrm{unbeamed}}$) of sources with known Doppler factors from Hovatta et al. (2009), but this hypothesis was ruled out. This is because a significant correlation was still found for a single sub-sample of sources. We have repeated the same test with our updated data set, and we have obtained no correlation between the L_{unbeamed} and m_{L} (Fig. 11) for neither the entire source sample, quasars, nor BL Lacs. This opens again the possibility to use orientation and relativistic effects to explain the reported L_{beamed} versus m_{L} anti-correlation, although other alternative explanations (e.g., Agudo et al. 2010) cannot be ruled out.

4.2.3. Linear polarization angle vs. jet position angle

Figure 12 shows the distribution of misalignment of the jet position angle (ϕ_{jet}, see Table 1) with the polarization (electric vector) position angle at 86 GHz (χ_{86}, see Table 2), this is, $|\chi_{86} - \phi_{\mathrm{jet}}|$, for the entire source sample, quasars, and BL Lacs. To give the most reliable estimate of ϕ_{jet} as possible to compare it with our millimeter polarimetric measurements, we first searched in the 86 GHz VLBI Survey by Lee et al. (2008) and then followed it by the 15 GHz data from the MOJAVE survey (Lister & Homan 2005, preferentially). A more exhaustive search from references 1 to 10 in Table 1 was done for every source not found in these two surveys. If a source was found in several references, we adopted the higher frequency ϕ_{jet} measurement.

Figure 12 shows a very weak (almost non-existent) trend for sources in our entire sample and quasars to distribute χ_{86} nearly parallel to ϕ_{jet} with $0° \leq |\chi_{86} - \phi_{\mathrm{jet}}| \lesssim 30°$. A similar result was also shown in Agudo et al. (2010). BL Lacs seem to show a different $|\chi_{86} - \phi_{\mathrm{jet}}|$ distribution, although also with an additional (but also very weak) excess of sources, where χ_{86} is almost parallel to ϕ_{jet}. However, our Kolmogorov-Smirnov (K-S) tests give a too weak confidence on the hypothesis that our entire source sample and quasars come from a different parent distribution than BL Lacs (12% and 23%, respectively). Therefore, it is not possible to confirm this difference. Our 229 GHz linear polarization angle measurements give similar results (Fig. 13). We also report a very weak trend for the 229 GHz polarization angle

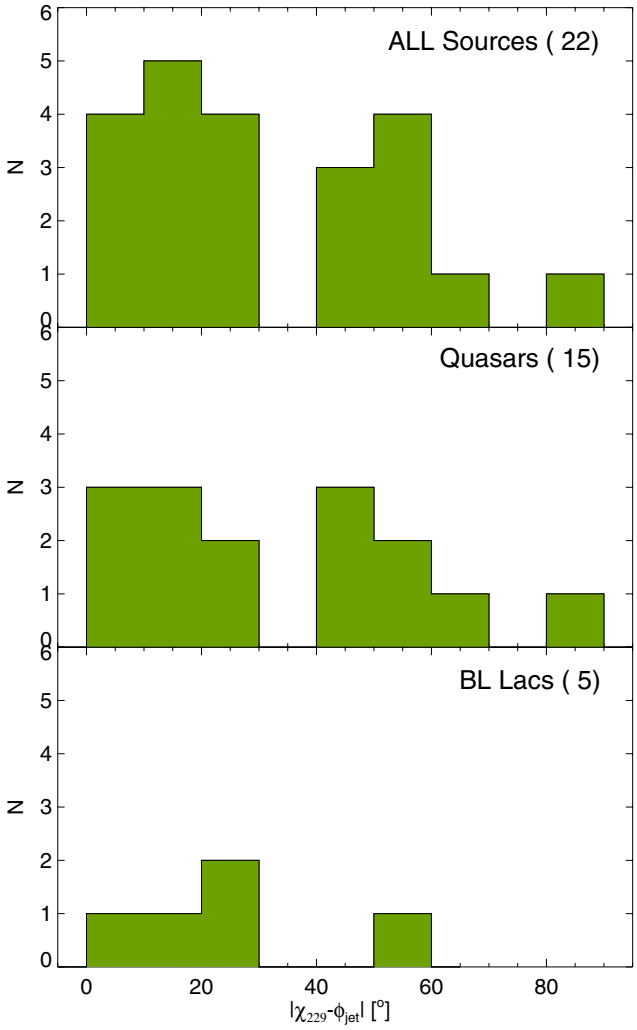

Fig. 13. Same as Fig. 12 but for 230 GHz linear polarization angle (χ_{230}) measurements.

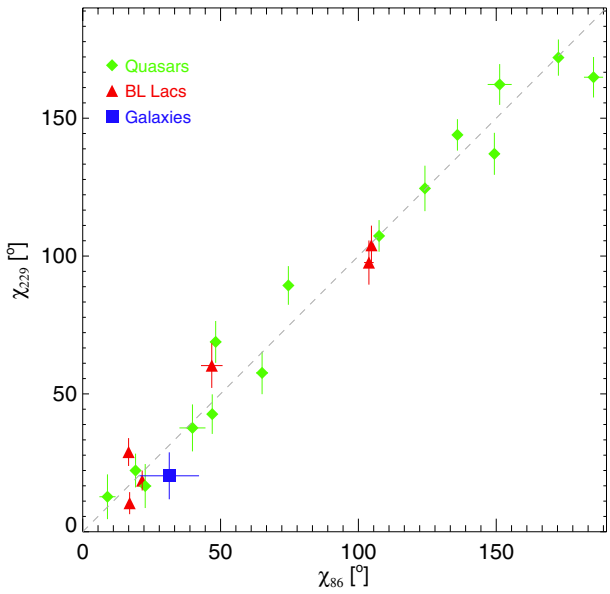

Fig. 14. 86 GHz linear polarization angle (χ_{86}) as compared to the simultaneously measured 229 GHz linear polarization angle (χ_{229}) for the 22 sources with detected polarization at both 86 and 229 GHz. The dashed line represents the $\chi_{86} = \chi_{229}$ line.

to distribute nearly parallel to the jet position angle for the entire source sample and quasars. The K-S test on their $|\chi_{229} - \phi_{\rm jet}|$ distributions give a 99.5% confidence to come from the same parent distribution. For BL Lacs, $|\chi_{229} - \phi_{\rm jet}|$ might be distributed in all possible misalignment angles, although the small number of sources in this case (Fig. 13) do not allow us to make any reliable statement or statistical tests.

Even for the case of the entire source sample considered for the $|\chi_{86} - \phi_{\rm jet}|$ histogram, the excess of sources accumulated toward $0° \leq |\chi_{86} - \phi_{\rm jet}| \lesssim 30°$ only represents 17% of the total number of sources in our entire sample, which gives an idea of the small relevance of this excess. Therefore, we fully confirm that there is no clear trend for the millimeter linear polarization angle to be aligned either parallel or perpendicular to $\phi_{\rm jet}$ for all source sub-samples considered here. This result contradicts theoretical expectations for *purely axisymmetric* jets, which predict that the polarization angle should be observed either parallel or perpendicular to the jet axis (e.g., Lyutikov et al. 2005; Cawthorne 2006). Moreover, several previous observational attempts to probe this bi-modality through observations at centimeter wavelengths (e.g., Gabuzda et al. 2000; Pollack et al. 2003; Lister & Homan 2005) do not agree among each other (see Agudo et al. 2010, for a summary on their differences).

There are three possible explanations for why our observations do not match the expectations from theory, namely, why we do not detect a clear trend of either quasars or BL Lacs to distribute their short millimeter polarization degree either parallel or perpendicular to the jet. These explanations are as follows: a) a larger χ variability amplitude and/or time scale at millimeter wavelengths with regard to those at longer centimeter wavelengths; b) different physical properties of the region where the bulk of the short millimeter emission is radiated (with regard to those at longer centimeter wavelengths); c) and significant departures from axisymmetric jet geometries and dynamics on the short millimeter emission regions that should show different expected integrated polarization angles than those for axisymmetric jets. Combinations of options a, b, and c are, of course, possible as well.

4.3. Faraday rotation between 86 and 229 GHz

In Fig. 14, we compare the linear polarization angle measured at 86 and 229 GHz for the 22 sources detected in polarization at both frequencies. The figure clearly shows that there is a general good match between χ_{86} and χ_{229} within the errors. Although there are some deviations from the $\chi_{86} = \chi_{229}$ line in Fig. 14, none of the points are away from this line at more than 3σ with regard to the χ_{229} measurement. The relatively large χ_{229} uncertainties, which are typically several times larger than those at 86 GHz, do not allow us to provide a $> 3\sigma$ measurement of Faraday rotation measure (RM)[7] for any of the sources with both 86 and 229 GHz polarization angle measurements. Instead, only a 3σ RM value, which is typically of the order of several times 10^4 rad m^2, is given in Table 2 for the 22 sources mentioned above. This result is consistent with previous expectations for rotation measures not much larger than RM $\sim 10^4$ rad m^{-2}, although we cannot rule out such large values with the available data. Large rotation measures have already been detected in some sources through ultra-high-resolution and

[7] RM $= (\chi_{\rm obs}(\lambda) - \chi_{\rm int})/\lambda^2$ with $\chi_{\rm int}$ being the intrinsic polarization angle and $\chi_{\rm obs}(\lambda)$ as the observed polarization angle at the observing wavelength λ.

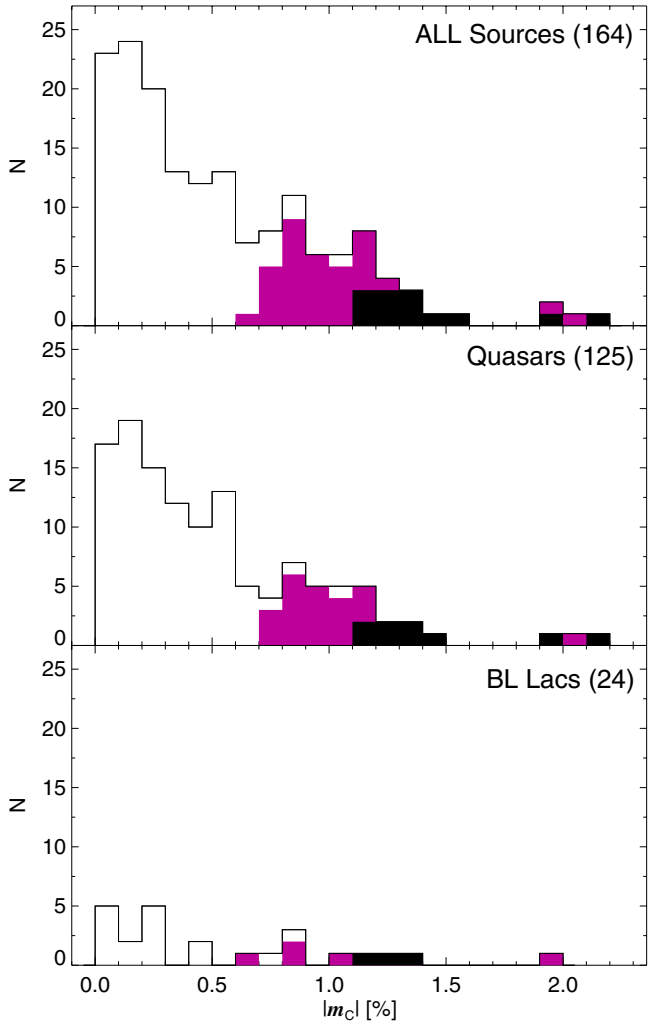

Fig. 15. Distribution of the absolute value of 86 GHz circular polarization for the entire source sample, quasars, and BL Lacs. Black areas correspond to $m_{C,86}$ detections at $\geq 3\sigma$. Violet shaded areas indicate observing results with $\geq 2\sigma$, whereas unshaded areas symbolize all m_C measurements, regardless of their significance.

high-precision polarimetric-VLBI observations (e.g., Attridge et al. 2005; Gómez et al. 2008, 2011; Agudo et al. 2012a).

5. Circular polarization

In Fig. 15, we present the distribution of the absolute value of 86 GHz circular polarization $|m_{C,86}|$ for the samples considered here. We show the distributions of $|m_{C,86}|$ detections at $\geq 3\sigma$ level (black), $|m_{C,86}|$ measurements at $\geq 2\sigma$ level (violet), and all $|m_{C,86}|$ measurements regardless of their significance (unshaded areas).

As expected from the previously known low level of circular polarization degree of blazars (typically $\lesssim 0.5\%$ at 2 cm Homan & Lister 2006), we only detect $m_{C,86}$ for a small fraction of sources (6%). This small detection rate is consistent with the one reported by Homan & Lister (2006) through 15 GHz VLBA observations (∼15%), and our own results for our previous survey (Agudo et al. 2010), where we only detected circular polarization at 86 GHz for eight sources (6% of the entire sample). No circular polarization was detected from our 229 GHz observations.

Figure 15 shows that most of the 13 circular polarization detections correspond to values in the range $0.9\% \lesssim |m_{C,86}| \lesssim 1.6\%$ (for sources 0229+131, 0430+052, 0451−282, 0716+714, 0917+449, 0954+658, 1324+224, 1328+307, 1642+690, 2131−021, and 2342−161), although there are two detections at $|m_{C,86}| \approx 2\%$ (for 0923+392 and 1124−186). These correspond to significantly larger $|m_{C,86}|$ values than those observed on our first survey (Agudo et al. 2010), where we only detected 86 GHz circular polarization in the range $0.3\% \lesssim |m_{C,86}| \lesssim 0.7\%$. Apart from variability, we do not have an explanation of why no large circular polarization values ($|m_{C,86}| \gtrsim 0.7\%$) were detected in our previous 86 GHz survey, although 8 sources detected in circular polarization in our new survey were also present in the sample of our previous survey.

Among all sources for which we detect 86 GHz circular polarization in our new survey, only one (1124−186 with $m_{C,86} = -1.98 \pm 0.35\%$) was also detected in the previous survey (with $m_{C,86} = 0.58 \pm 0.19\%$). We invoke circular polarization variability to explain this $m_{C,86}$ sign reversal and the large difference in $|m_{C,86}|$ between the observations of the two surveys in five years. This is consistent with circular polarization variability levels previously reported for radio-loud AGN (e.g., Aller et al. 2003).

Moreover, among all sources with detected $m_{C,86}$ in our new survey, only 0716+714 (with $m_{C,86} = -1.25 \pm 0.35\%$) was also detected by the MOJAVE team with $m_{C,15} = +0.37 \pm 0.11\%$, which is also consistent with models that can reproduce considerable m_C differences at different observing frequencies (e.g., Homan et al. 2009).

6. Total flux and linear polarization variability

In Fig. 16, we compare the 86 GHz total flux density from the first 3.5 mm AGN Polarimetric Survey in Agudo et al. (2010) and the measurements presented in this paper using the 86 GHz total flux variability ratio ($RS_{86}^{\rm var}$)[8]. The figure clearly shows a large level of variability by a median factor of ∼1.5 for the entire source sample at time scales $\lesssim 5$ years and with 19% of sources displaying S_{86} variations by a factor >2. No significant difference in the $RS_{86}^{\rm var}$ distribution is found between any of the different samples considered in Fig. 16.

The distribution of the 86 GHz polarization degree variability ratio ($Rm_{L,86}^{\rm var}$)[9] is shown in Fig. 17. This Figure also points out an even larger degree of variability of $m_{L,86}$ with a median variability factor $Rm_{L,86}^{\rm var} = 1.7$ and with 34% of the sources displaying an increased (or decreased) $m_{L,86}$ by a factor of 2 on the time scale of years. We obtain similar results for the different sub-samples considered in Fig. 17. Note that $RS_{86}^{\rm var}$ and $Rm_{L,86}^{\rm var}$ are not correlated (Spearman's $\rho = 0.17$ with 21.1% confidence), hence reflecting the complicated time dependent behavior of different blazars studied in detail (e.g., Marscher et al. 2010; Jorstad et al. 2010; Agudo et al. 2011a,b; Wehrle et al. 2012).

The 86 GHz linear polarization angle is also highly variable on the time scale of years, as shown by Fig. 18, where we present the distribution of the absolute difference for the 86 GHz polarization angle from Agudo et al. (2010) and ($\Delta\chi_{86}^{\rm var}$)[10] for the entire source sample, quasars, BL Lacs, and radio galaxies in this

[8] $RS_{86}^{\rm var} = \frac{\max(S_{86}^{\rm Agudo\ et\ al.\ (2010)}, S_{86}^{\rm this\ paper})}{\min(S_{86}^{\rm Agudo\ et\ al.\ (2010)}, S_{86}^{\rm this\ paper})}$.

[9] $Rm_{L,86}^{\rm var} = \frac{\max(m_{L,86}^{\rm Agudo\ et\ al.\ (2010)}, m_{L,86}^{\rm this\ paper})}{\min(m_{L,86}^{\rm Agudo\ et\ al.\ (2010)}, m_{L,86}^{\rm this\ paper})}$.

[10] $\Delta\chi_{86}^{\rm var} = |\chi_{86}^{\rm Agudo\ et\ al.\ (2010)} - \chi_{86}^{\rm this\ paper}|$.

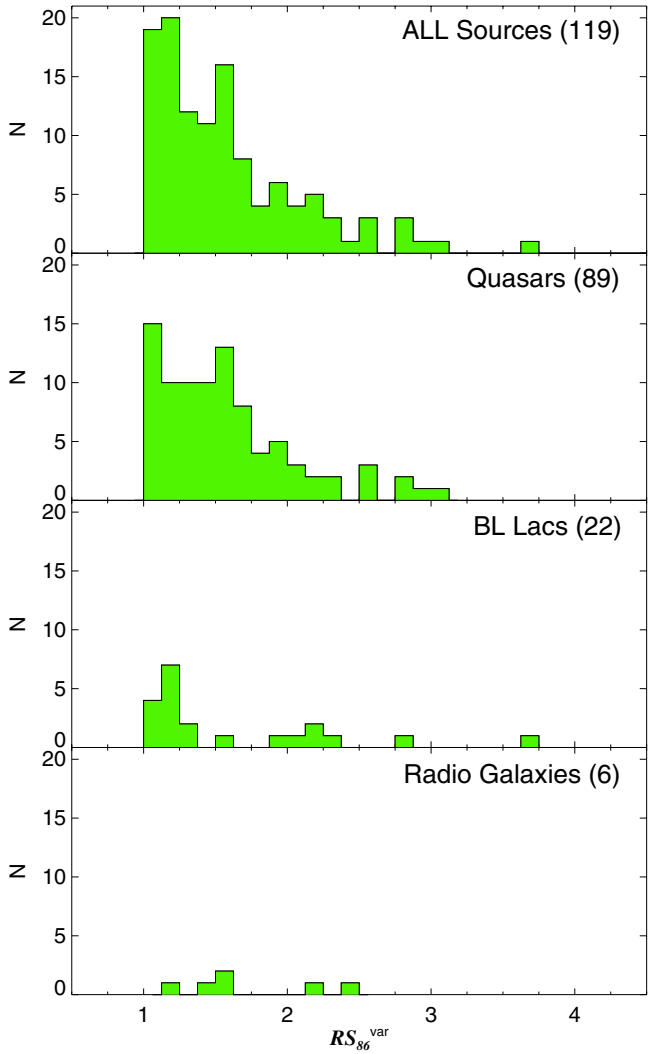

Fig. 16. Distribution of 86 GHz total flux variability ratio (RS_{86}^{var}, see the text) for the entire source sample, quasars, BL Lacs, and radio galaxies. One source (0422+004) with $RS_{86}^{var} = 6.3$ is out of scale.

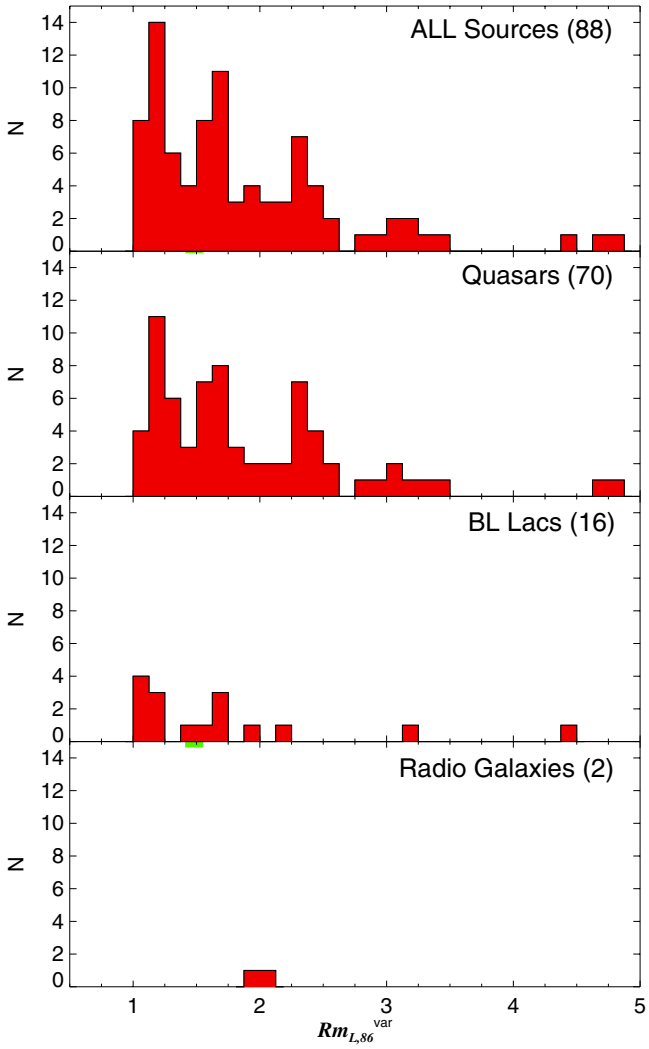

Fig. 17. Distribution of 86 GHz polarization degree variability ratio ($Rm_{L,86}^{var}$, see the text) for the entire source sample, quasars, BL Lacs, and radio galaxies.

paper. Figure 18 also shows that the difference of 86 GHz linear polarization angle of blazars on the time scale of years is essentially evenly distributed among all possible angles between 0° and 90°, except for a small fraction (14%) of sources that tend to conserve the same polarization angle in such time scales. There is a 90.2% probability for the quasar and the BL Lac distributions in Fig. 18 to come from different parent distributions, but this is not enough for us to claim a statistically significant difference between them with regard to the behavior of their polarization angle variability.

Radio-loud AGN, and blazars, in particular, are able to show extreme total flux density variability in the millimeter range (and in other spectral ranges) by up to one order of magnitude on a time scale from months (Jorstad et al. 2005; Teräsranta et al. 2005; Fuhrmann et al. 2008) to days (Agudo et al. 2006). Such extreme variability (enhanced by relativistic Doppler boosting) is often connected to the ejection and propagation of strong jet perturbations (blobs or shocks) from the innermost regions of the source (e.g., Jorstad et al. 2005, 2010; Kadler et al. 2008; Perucho et al. 2008; Marscher et al. 2010; Agudo et al. 2011a,b). Regarding linear polarization variability at short millimeter wavelengths, blazars have been shown to display $m_{\rm L}$ excursions up to one order of magnitude and χ rotations that are >90° on time scales of months or even weeks (e.g. Jorstad et al. 2005, 2010; D'Arcangelo et al. 2007, 2009; Agudo et al. 2011a,b). It is thus not surprising that a large level of variability affects our results and, of course, the completeness of our sample (see Sect. 2). The expected influence of such variability in our study is to broaden the S, $m_{\rm L}$, and χ distributions or to hide their correlation with other variables – hence, making it more difficult to obtain statistically significant relations – but never faking results to give unrealistic correlations. We are therefore confident on the significance of the results shown here.

7. Summary

We have presented the first simultaneous 3.5 and 1.3 mm polarization survey of radio-loud AGN on a large sample of 211 sources, which are dominated by blazars.

Our total flux measurements show that almost all measured sources (96%) have a spectral index $\tilde{\alpha}^{\rm Q}_{86,229} < 0$. Most of them have an optically thin spectrum, between 86 and 229 GHz with median spectral indexes $\tilde{\alpha}^{\rm Q}_{86,229} = -0.75$ for quasars and $\tilde{\alpha}^{\rm B}_{86,229} = -0.56$ for BL Lacs. In contrast, the 15 to 86 GHz

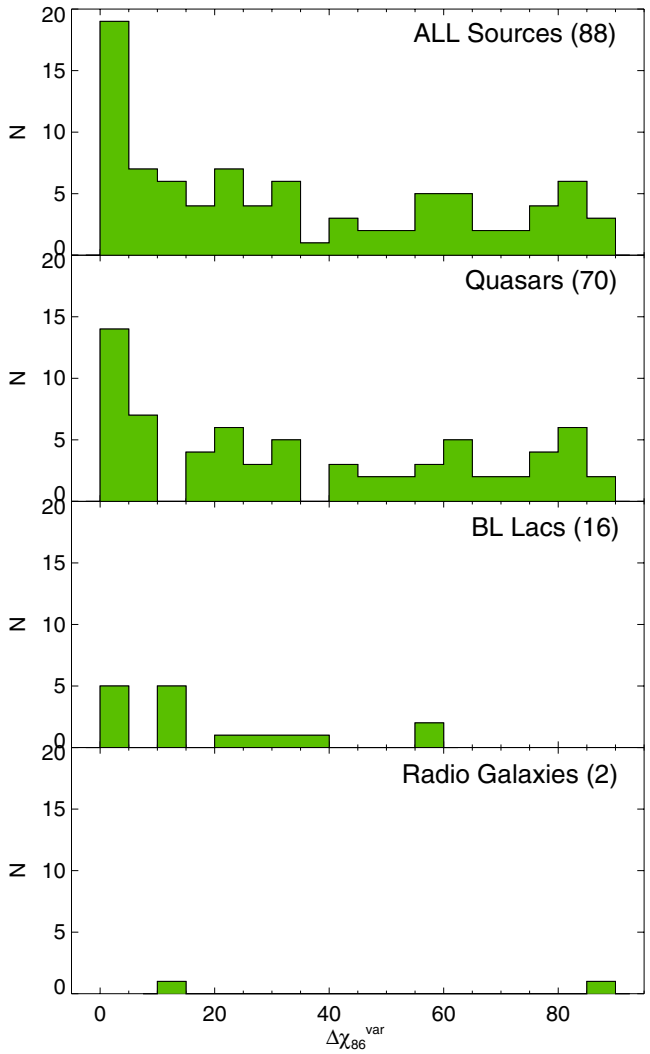

Fig. 18. Distribution of the absolute difference of the 86 GHz polarization angle in Agudo et al. (2010) and in this paper ($\Delta\chi_{86}^{var}$, see the text) for the entire source sample, quasars, BL Lacs and radio galaxies.

spectral index is distributed toward flatter and mild optically-thin spectral indices for both quasars and BL Lacs.

We detect a linear polarization above 3σ levels for 88% and 13% of the sources detected at 86 and 229 GHz, respectively. We find that the median linear polarization degrees of quasars and BL Lacs are different at 86 GHz and 229 GHz: $\tilde{m}^{Q}_{L,86} = 3.2\%$ and $\tilde{m}^{Q}_{L,229} = 7.7\%$ for quasars and $\tilde{m}^{B}_{L,86} = 4.6\%$ and $\tilde{m}^{B}_{L,229} = 10.2\%$ for BL Lacs. The difference between the quasar and BL Lac m_L distributions at 86 GHz is significant to a 97.1% confidence level. This difference is consistent with recent work suggesting that quasars have, in general, smaller viewing angles than BL Lacs. This follows the assumption that the magnetic fields in the jets of BL Lacs and quasars are not homogeneously distributed along the jet axis or that the jets themselves are not axisymmetric.

We show for the first time that the 229 GHz linear polarization degree is in general a factor ~1.6 larger than the one at 86 GHz. We also confirm that the 86 GHz polarization degree is stronger than that at 15 GHz by a factor of ~1.6. We observed a good match between the measured polarization angles at 86 and 229 GHz for 22 sources. Therefore, at these wavelengths, it is unlikely to expect significant Faraday depolarization effects. As a result, the stronger linear polarization degree at higher frequencies suggests that the magnetic field is progressively better ordered in blazar jet regions that are located progressively upstream in the jet.

An anti-correlation between the millimeter luminosity and the linear polarization degree is confirmed here for the entire source sample and quasars at 86 GHz. We attribute this relation to purely relativistic and orientation effects. That is, sources whose jets are better oriented to the line of sight display larger luminosities (because of their larger Doppler boosting) and also lower linear polarization degrees (because orthogonal polarization components are cancelled along the line of sight).

Unlike theoretical predictions from axially symmetric jet models, we show an essentially non-existent relation between χ_{86} and the jet structural position angle for both quasars and BL Lacs for distributing at a preferential misalignment angle (see also Agudo et al. 2010). Only a small 17% of quasars tend to have $0^\circ \leq |\chi_{86} - \phi_{jet}| \lesssim 30^\circ$. This result seems to be reproduced also at 229 GHz, although the small number of sources detected in polarization at this frequency do not allow us to obtain robust conclusions. These results imply that either the magnetic field or the emitting particle distributions (or both) that are responsible for the synchrotron radiation in the innermost regions where the short mm emission is radiated in blazars, have a markedly non axisymmetric character in general.

Comparison of our data with the 86 GHz measurements presented in Agudo et al. (2010) shows a considerable high total flux variability factor (RS^{var}_{86}) with median variations of $\bar{RS}^{var}_{86} \sim 1.5$ on the time scale of years, where a 19% of sources show $RS^{var}_{86} \gtrsim 2$ and even one source (0422+004) experiences extreme total flux variations by $RS^{var}_{86} = 6.3$. The 86 GHz linear polarization degree is also equally highly variable with a median variability factor $\bar{Rm}^{var}_{L,86} \sim 1.7$ and with 34% of the sources displaying $Rm^{var}_{L,86} \gtrsim 2$ with maximum variations by a factor of ~5. The 86 GHz linear polarization angle is also highly variable on the time scale of years. Except for a small fraction (14%) of sources that tend to conserve the same polarization angle, most sources show drastically different polarization angles that are evenly distributed among all possible angles between 0° and 90° at such time scales.

Acknowledgements. The authors acknowledge the anonymous referee for his/her constructive revision of this paper, which allowed us to improve it considerably. This paper is based on observations carried out with the IRAM 30 m telescope. IRAM is supported by INSU/CNRS (France), MPG (Germany) and IGN (Spain). The research at the IAA-CSIC is supported in part by the Ministerio de Ciencia e Innovación of Spain, and by the regional government of Andalucía through grants AYA2010-14844 and P09-FQM-4784, respectively. The research at Boston University was funded by US National Science Foundation grant AST-0907893, NASA grants NNX08AJ64G, NNX08AU02G, NNX08AV61G, and NNX08AV65G, and NRAO award GSSP07-0009. This research has made use of the NASA/IPAC Extragalactic Database, the MOJAVE database (Lister et al. 2009), the one by the Blazar Research Group at the Boston University, as well as the USNO Radio Reference Frame Image Database.

References

Ackermann, M., Ajello, M., Baldini, L., et al. 2010, ApJ, 721, 1383
Ackermann, M., Ajello, M., Allafort, A., et al. 2011, ApJ, 743, 171
Acosta-Pulido, J. A., Agudo, I., Barrena, R., et al. 2010, A&A, 519, A5
Agudo, I., Krichbaum, T. P., Ungerechts, H., et al. 2006, A&A, 456, 117
Agudo, I., Bach, U., Krichbaum, T. P., et al. 2007, A&A, 476, L17
Agudo, I., Thum, C., Wiesemeyer, H., & Krichbaum, T. P. 2010, ApJS, 189, 1
Agudo, I., Jorstad, S. G., Marscher, A. P., et al. 2011a, ApJ, 726, L13
Agudo, I., Marscher, A. P., Jorstad, S. G., et al. 2011b, ApJ, 735, L10
Agudo, I., Gómez, J. L., Casadio, C., Cawthorne, T. V., & Roca-Sogorb, M. 2012a, ApJ, 752, 92
Agudo, I., Marscher, A. P., Jorstad, S. G., et al. 2012b, ApJ, 747, 63
Aller, H. D., Aller, M. F., & Plotkin R. M. 2003, ApSS, 288, 17

Attridge, J. M., Wardle, J. F. C., & Homan, D. C. 2005, ApJ, 633, L85
Bach, U., Villata, M., Raiteri, C. M., et al. 2006, A&A, 456, 105
Blandford, R. D., & Payne, D. G. 1982, MNRAS, 199, 883
Carter, M., Lazareff, B., Maier, D., et al. 2012, A&A, 538, A89
Cawthorne, T. V. 2006, MNRAS, 367, 851
Cohen, R. D., Smith, H. E., Junkkarinen, V. T., & Burbidge, E. M. 1987, ApJ, 318, 577
D'Arcangelo, F. D., Marscher, A. P., Jorstad, S. G., et al. 2007, ApJ, 659, L107
D'arcangelo, F. D., Marscher, A. P., Jorstad, S. G., et al. 2009, ApJ, 697, 985
de Vaucouleurs, G., de Vaucouleurs, A., Corvin, H. G., et al. 1991, Third Reference Catalogue of Bright Galaxies. (New York: Springer)
Fuhrmann, L., Krichbaum, T. P., Witzel, A., et al. 2008, A&A, 490, 1019
Gehan, E. A. 1965, Biometrika, 52, 203
Gabuzda, D. C., Pushkarev, A. B., & Cawthorne, T. V. 2000, MNRAS, 319, 1109
Giommi, P., Padovani, P., & Polenta, G. 2013, MNRAS, 431, 1914
Gold, B., Odegard, N., Weiland, J. L., et al. 2011, ApJS, 192, 15
Gómez, J. L., Marscher, A. P., Alberdi, A., Jorstad, S. G., & Agudo, I. 2001, ApJ, 561, L161
Gómez, J. L., Marscher, A. P., Jorstad, S. G., Agudo, I., & Roca-Sogorb, M. 2008, ApJ, 681, L69
Gómez, J. L., Roca-Sogorb, M., Agudo, I., Marscher, A. P., & Jorstad, S. G. 2011, ApJ, 733, 11
Healey, S. E., Romani, R. W., Cotter, G., et al. 2008, ApJS, 175, 97
Homan, D. C., & Lister, M. L. 2006, AJ, 131, 1262
Homan, D. C., Lister, M. L., Aller, H. D., Aller, M. F., & Wardle, J. F. C. 2009, ApJ, 696, 328
Hovatta, T., Valtaoja, E., Tornikoski, M., & Lähteenmäki, A. 2009, A&A, 494, 527
Jorstad, S. G., Marscher, A. P., Lister, M. L., et al. 2005, AJ, 130, 1418
Jorstad, S. G., Marscher, A. P., Stevens, J. A., et al. 2007, AJ, 134, 799
Jorstad, S. G., Marscher, A. P., Larionov, V. M., et al. 2010, ApJ, 715, 362
Kadler, M., Ros, E., Lobanov, A. P., Falcke, H., & Zensus, J. A. 2004, A&A, 426, 481
Kadler, M., Ros, E., Perucho, M., et al. 2008, ApJ, 680, 867
Lavalley, M., Isobe, T., & Feigelson, E. 1992, in Astronomical Data Analysis Software and Systems I, eds. D. M. Worrall, C. Biemesderfer, & J. Barnes (ASP: San Francisco), ASP Conf. Ser., 25, 245
Lawrence, C. R., Pearson, T. J., Readhead, A. C. S., & Unwin, S. C. 1986, AJ, 91, 494
Lee, S.-S., Lobanov, A. P., Krichbaum, T. P., et al. 2008, AJ, 136, 159
Lister, M. L., & Homan, D. C. 2005, AJ, 130, 1389
Lister, M. L., Aller, H. D., Aller, M. F., et al. 2009, AJ, 137, 3718
Lyutikov, M., Pariev, V. I., & Gabuzda, D. C. 2005, MNRAS, 360, 869
Marscher, A. P., & Gear, W. K. 1985, ApJ, 298, 114
Marscher, A. P., Jorstad, S. G., Larionov, V. M., et al. 2010, ApJ, 710, L126
Nilsson, K., Pursimo, T., Sillanpää, A., Takalo, L. O., & Lindfors, E. 2008, A&A, 487, L29
Perucho, M., Agudo, I., Gómez, J. L., et al. 2008, A&A, 489, L29
Pollack, L. K., Taylor, G. B., & Zavala, R. T. 2003, ApJ, 589, 733
Pushkarev, A. B., Kovalev, Y. Y., Lister, M. L., & Savolainen, T. 2009, A&A, 507, L33
Rybicki, G. B., & Lightman, A. P. 1979, Rad. Process. Astrophys. (New York: Wiley Interscience)
Sbarufatti, B., Treves, A., & Falomo, R. 2005, ApJ, 635, 173
Sowards-Emmerd, D., Romani, R. W., Michelson, P. F., Healey, S. E., & Nolan, P. L. 2005, ApJ, 626, 95
Tavecchio, F., Ghisellini, G., Bonnoli, G., & Ghirlanda, G. 2010, MNRAS, 405, L94
Teräsranta, H., Wiren, S., Koivisto, P., Saarinen, V., & Hovatta, T. 2005, A&A, 440, 409
Thum, C., Wiesemeyer, H., Paubert, G., Navarro, S., & Morris, D. 2008, PASP, 120, 777
Urry, C. M., & Padovani, P. 1995, PASP, 107, 803
Véron-Cetty, M.-P., & Véron, P. 2006, A&A, 455, 773
Wehrle, A. E., Marscher, A. P., Jorstad, S. G., et al. 2012, ApJ, 758, 72
Zavala, R. T., & Taylor, G. B. 2004, ApJ, 612, 749

Pages 14 to 22 are available in the electronic edition of the journal at http://www.aanda.org

Table 1. Source properties.

Source name (IAU) (1)	Alias (2)	(J2000.0) (3)	(J2000.0) (4)	z (5)	Cl. (6)	V mag (7)	$\phi_{\rm jet}$ [°] (8)	$\nu_{\rm obs}$ [GHz] (9)	Ref. ($\phi_{\rm jet}$) (10)	*Fermi* 2LAC? (11)
0003+380	S4 0003+38	00 05 57.1754	+38 20 15.148	0.229	G	19.9	106	15	9	Y
0003-066	NRAO 5	00 06 13.8928	–06 23 35.334	0.347	B	18.5	181	86	6	...
0007+106	III Zw 2	00 10 31.0058	+10 58 29.504	0.089	G	15.4	221	86	6	...
0017+200	PKS 0017+200	00 19 37.8545	+20 21 45.644	...	B	20.6	305	43	10	...
0027+056	PKS 0027+056	00 29 45.8962	+05 54 40.712	1.317	Q	15.9	163	15	9	...
0035-252	PKS 0035-252	00 38 14.7354	–24 59 02.235	1.196	Q	20.7	316	8	10	Y
0045-255	NGC 253	00 47 33.120	–25 17 17.59	0.001	G	14.0	...	...	...	Y
0048-097[a]	PKS 0048-09	00 50 41.3173	–09 29 05.209	0.635	B	17.4	7	86	6	Y
0048-071	PKS 0048-071	00 51 08.2098	–06 50 02.228	1.975	Q	19.5	...	...	...	Y
0055+300	NGC 0315	00 57 48.8833	+30 21 08.812	0.016	G	12.5	308	15	5	...
0059+581[b]	TXS 0059+581	01 02 45.7623	+58 24 11.136	0.644	Q	17.3	235	15	8	y
0106+013	PKS 0106+01	01 08 38.7710	+01 35 00.317	2.107	Q	18.4	235	15	8	Y
0112-017	PKS 0112-017	01 15 17.0999	–01 27 04.576	1.365	Q	17.5	118	15	5	...
0113-118	PKS 0113-11	01 16 12.5219	–11 36 15.432	0.672	Q	19.0	338	15	9	Y
0119+115	PKS 0119+11	01 21 41.5950	+11 49 50.413	0.570	Q	19.7	10	15	8	...
0122-003	PKS 0122-00	01 25 28.8438	–00 05 55.932	1.070	Q	16.7	265	15	9	...
0130-171	PKS 0130-17	01 32 43.4874	–16 54 48.522	1.020	Q	18.4	262	15	9	Y
0133+476	DA 55	01 36 58.5947	+47 51 29.100	0.859	Q	19.5	334	86	6	Y
0135-247	PKS 0135-247	01 37 38.3463	–24 30 53.884	0.835	Q	17.3	75	5	3	Y
0146+056	PKS 0146+056	01 49 22.3709	+05 55 53.569	2.345	Q	20.1	111	15	10	...
0149+218	PKS 0149+21	01 52 18.0590	+22 07 07.700	1.320	Q	19.4	344	15	5	...
0202+149[c]	PKS 0202+14	02 04 50.4139	+15 14 11.043	0.405	Q	21.0	338	15	8	Y
0202+319	DW 0202+31	02 05 04.9253	+32 12 30.095	1.466	Q	17.4	65	86	6	Y
0215+015	PKS 0215+015	02 17 48.9547	+01 44 49.699	1.715	Q	16.1	105	15	8	Y
0212+735	S5 0212+73	02 17 30.8132	+73 49 32.621	2.367	Q	20.0	113	86	6	y
0218+357	S4 0218+35	02 21 05.4701	+35 56 13.722	0.944	Q	20.0	68	5	3	Y
0220+427	3C 66.0B	02 23 11.4112	+42 59 31.384	0.021	G	14.8	...	...	...	...
0224+671[d]	4C +67.05	02 28 50.0514	+67 21 03.029	0.523	Q	19.5	4	15	8	...
0229+131	PKS 0229+13	02 31 45.8940	+13 22 54.716	2.065	Q	17.7	63	15	9	...
0234+285	B2 0234+28	02 37 52.4056	+28 48 08.990	1.207	Q	19.3	283	15	8	Y
0235+164[e]	AO 0235+164	02 38 38.9301	+16 36 59.275	0.940	B	20.9	270	86	6	Y
0256-005	PKS 0256-005	02 59 28.5161	–00 19 59.974	1.995	Q	17.6	...	...	...	...
0305+039	NGC 1218	03 08 26.2238	+04 06 39.300	0.029	G	13.9	59	15	9	...
0306+102	PKS 0306+102	03 09 03.6235	+10 29 16.341	0.862	Q	18.4	44	8	3	Y
0316+413	3C 84	03 19 48.1601	+41 30 42.106	0.017	G	12.5	186	86	6	Y
0327-241	PKS 0327-241	03 29 54.0755	–23 57 08.773	0.895	Q	19.4	...	...	...	...

Notes. Columns are as follows: (1) IAU B1950.0 source name; (2) source name in other catalogs; (3) and (4) J2000.0 observing right ascension and declination; (5) redshift from Véron-Cetty & Véron (2006); (6) optical classification from Véron-Cetty & Véron (2006); (7) V magnitude from Véron-Cetty & Véron (2006); (8) jet position angle ($\phi_{\rm jet}$); (9) VLBI observing frequency for the image from which $\phi_{\rm jet}$ was obtained; (10) References from which $\phi_{\rm jet}$ was obtained (see below); (11) *Fermi*-2LAC source (Y = yes, y = yes but not in the clean list).

References. (1) Agudo et al. (2007); (2) BU- Blazar Group Web Page; (3) Fomalont et al. (2000); (4) Jorstad et al. (2005); (5) Kellermann et al. (2004); (6) Lee et al. (2008); (7) Lister et al. (2001); (8) Lister & Homan (2005); (9) MOJAVE Web Page; (10) USNO Radio Reference Frame Image Database Web Page; (11) Xu et al. (1995). [a] Redshift from Ackermann et al. (2011). [b] V-mag = R-mag from NED. Not present in Véron-Cetty & Véron (2006) catalog. Redshift from Sowards-Emmerd et al. (2005). [c] Classified as a possible galaxy in Véron-Cetty & Véron (2006) catalog. [d] V-mag = optical-mag from NED. Not present in Véron-Cetty & Véron (2006) catalog. Redshift from Sowards-Emmerd et al. (2005). [e] V-mag = optical-mag from NED. Redshift from Cohen et al. (1987). Classified as a possible galaxy in Véron-Cetty & Véron (2006) catalog. [f] From Agudo et al. (2007) and Acosta-Pulido et al. (2010). [g] Not present in Véron-Cetty & Véron (2006) catalog. [h] V-mag = optical-mag from NED. Not present in Véron-Cetty & Véron (2006) catalog. Redshift from Sowards-Emmerd et al. (2005). [i] Not present in Véron-Cetty & Véron (2006) catalog. [j] Not present in Véron-Cetty & Véron (2006) catalog. Redshift, R-mag = optical-mag and optical identification from Healey et al. (2008). [k] Not present in Véron-Cetty & Véron (2006) catalog. [l] Redshift from Nilsson et al. (2008). [m] Classified as a Galaxy on Véron-Cetty & Véron (2006) catalog. [n] z = 0.245 from Britzen et al. (in prep.). Sbarufatti et al. (2005) give $z > 0.75$. [o] Classified as a possible BL Lac in Véron-Cetty & Véron (2006) catalog. [p] Not present in Véron-Cetty & Véron (2006) catalog. Redshift, classification and R-mag = optical-mag from de Vaucouleurs et al. (1991). [q] Not present in Véron-Cetty & Véron (2006) catalog. Redshift, R-mag = optical-mag and optical identification from Healey et al. (2008). [r] V-mag = optical-mag from NED, not present in Véron-Cetty & Véron (2006) catalog. [s] Not present in Véron-Cetty & Véron (2006) catalog. [t] Classified as a galaxy on Véron-Cetty & Véron (2006) catalog. [u] Redshift from Ackermann et al. (2011). [v] Classified as a quasar on Véron-Cetty & Véron (2006) catalog. [w] Not present in Véron-Cetty & Véron (2006) catalog. Redshift, R-mag = optical-mag and optical identification from Healey et al. (2008). [x] Classified as a quasar on Véron-Cetty & Véron (2006) catalog. [y] V-mag = R-mag from NED, not present in Véron-Cetty & Véron (2006) catalog. Redshift from Lawrence et al. (1986). [z] V-mag = R-mag from NED, not present in Véron-Cetty & Véron (2006) catalog. [a] V-mag = R-mag from NED, possible BLLac in Véron-Cetty & Véron (2006) catalog. [b] Classified as a quasar on Véron-Cetty & Véron (2006) catalog. [c] Not present in Véron-Cetty & Véron (2006) catalog. Redshift, R-mag = optical-mag and optical identification from Healey et al. (2008). [d] Not present in Véron-Cetty & Véron (2006) catalog. Redshift, R-mag = optical-mag and optical identification from Healey et al. (2008).

Table 1. continued.

Source name (IAU) (1)	Alias (2)	(J2000.0) (3)	(J2000.0) (4)	z (5)	Cl. (6)	V mag (7)	$\phi_{\rm jet}$ [°] (8)	$\nu_{\rm obs}$ [GHz] (9)	Ref. ($\phi_{\rm jet}$) (10)	*Fermi* 2LAC? (11)
0336-019	CTA 26	03 39 30.9377	–01 46 35.803	0.852	Q	18.4	74	86	6	Y
0338-214	PKS 0338-214	03 40 35.6078	–21 19 31.171	0.223	B	17.1	231	8	10	Y
0346-163	PKS 0346-163	03 48 39.2707	–16 10 17.752	...	B	18.0	...	...	...	...
0356+102	3C 98.0	03 58 54.43	+10 26 03.0	0.031	G	15.4	...	...	...	...
0355+508[f]	NRAO 150	03 59 29.7472	+50 57 50.161	1.517	Q	22.9	161	43	1	...
0403-132	PKS 0403-13	04 05 34.0033	–13 08 13.691	0.571	Q	17.1	179	15	8	Y
0415+379	3C 111	04 18 21.2772	+38 01 35.800	0.049	G	18.1	68	86	6	...
0420-014	PKS 0420-01	04 23 15.8007	–01 20 33.064	0.915	Q	17.0	192	86	6	Y
0422+004	PKS 0422+00	04 24 46.8420	+00 36 06.329	...	B	17.0	4	15	8	Y
0430+052	3C 120	04 33 11.0955	+05 21 15.620	0.033	G	15.1	244	86	6	...
0440-003	PKS 0440-00	04 42 38.6607	–00 17 43.418	0.844	Q	19.2	184	86	6	Y
0451-282	PKS 0451-28	04 53 14.6467	–28 07 37.327	2.560	Q	18.2	8	15	9	Y
0454-234	PKS 0454-234	04 57 03.1792	–23 24 52.018	1.003	Q	18.9	205	15	9	Y
0458-020	PKS 0458-02	05 01 12.8098	–01 59 14.255	2.291	Q	18.1	312	15	8	Y
0516-054[g]	WMAP 116	05 19 19.1	–05 40 40	...	U	...	...	...	...	...
0528+134	PKS 0528+134	05 30 56.4167	+13 31 55.150	2.070	Q	20.0	75	86	6	Y
0529+075[h]	CGRaBS J0532+0732	05 32 38.9984	+07 32 43.345	1.254	Q	19.0	322	15	8	Y
0548+378[i]	B3 0548+378A	05 51 58.7017	+37 51 07.435	...	U	...	...	...	...	...
0552+398	DA 193	05 55 30.8056	+39 48 49.165	2.363	Q	18.3	288	15	8	...
0605-085	OH-010	06 07 59.6992	–08 34 49.977	0.872	Q	17.6	132	15	8	Y
0607-157	PKS 0607-15	06 09 40.9494	–15 42 40.671	0.324	Q	18.0	189	86	6	...
0627-199	PKS 0627-199	06 29 23.7618	–19 59 19.723	...	B	18.6	8	15	9	Y
0631-223[j]	CGRaBS J0633-2223	06 33 26.7533	–22 23 22.353	1.508	Q	18.3	...	...	...	...
0642+449	OH 471	06 46 32.0259	+44 51 16.590	3.408	Q	18.5	93	86	6	...
0646-176	MC 0646-176	06 48 28.4985	–17 44 05.440	1.232	Q	19.9	...	...	...	y
0650+273[k]	WMAP J0652-2739	06 52 23.6	–27 39 04	...	U	...	...	...	...	...
0716+714[l]	S5 0716+71	07 21 53.4484	+71 20 36.363	0.310	B	15.5	35	15	8	Y
0723-008	PKS 0723-008	07 25 50.6399	–00 54 56.543	0.127	B	18.0	318	15	9	y
0727-115	PKS 0727-11	07 30 19.1124	–11 41 12.599	1.591	Q	20.3	254	15	8	y
0730+504	S4 0730+50	07 33 52.5205	+50 22 09.062	0.720	Q	19.3	224	15	8	Y
0735+178	PKS 0735+17	07 38 07.3937	+17 42 18.998	>0.424	B	16.2	59	86	6	Y
0736+017	PKS 0736+01	07 39 18.0338	+01 37 04.619	0.191	Q	16.5	275	86	6	Y
0738+313	OI 363	07 41 10.7033	+31 12 00.229	0.630	Q	16.9	192	86	6	...
0745+241[m]	PKS 0745+241	07 48 36.1092	+24 00 24.110	0.409	Q	19.6	296	15	5	...
0748+126	PKS 0748+126	07 50 52.0457	+12 31 04.829	0.889	Q	18.7	77	86	6	Y
0754+100	PKS 0754+100	07 57 06.6429	+09 56 34.852	0.266	B	15.0	15	15	8	Y
0805-077	PKS 0805-07	08 08 15.5360	–07 51 09.885	1.837	Q	19.8	341	15	8	Y
0814+425[n]	B3 0814+425	08 18 15.9996	+42 22 45.415	0.245	B	18.2	91	15	8	y
0820+225	PKS 0820+22	08 23 24.7591	+22 23 03.288	0.951	Q	19.5	37	5	3	...
0821+394	B2 0821+39	08 24 55.4830	+39 16 41.912	1.216	Q	18.2	314	15	9	Y
0823+033	PKS 0823+033	08 25 50.3383	+03 09 24.521	0.506	B	16.8	87	86	6	Y
0823-223	PKS 0823-223	08 26 01.5729	–22 30 27.202	>0.910	B	16.2	166	15	9	y
0827+243	S3 0827+24	08 30 52.0861	+24 10 59.821	0.939	Q	17.3	127	15	8	Y
0834-201	PKS 0834-20	08 36 39.2152	–20 16 59.503	2.752	Q	18.5	233	15	9	...
0838+133	3C 207.0	08 40 47.5884	+13 12 23.564	0.684	Q	18.1	83	15	9	Y
0836+710	S5 0836+71	08 41 24.3652	+70 53 42.173	2.218	Q	17.3	221	15	8	Y
0845-068[o]	TEX 0845-068	08 47 56.7372	-07 03 16.902	...	B	16.4	...	...	...	Y
0851+202	OJ 287	08 54 48.8749	+20 06 30.641	0.306	B	15.4	241	86	6	Y
0859-140	PKS 0859-14	09 02 16.8308	–14 15 30.873	1.339	Q	16.6	157	15	5	...
0906+015	PKS 0906+01	09 09 10.0915	+01 21 35.618	1.018	Q	17.3	51	15	8	Y
0912+029	PKS 0912+029	09 14 37.9134	+02 45 59.246	0.427	G	19.8	4	24	10	...
0915-118	3C 218	09 18 05.669	–12 05 43.95	0.054	G	14.8	...	...	...	...
0917+449	S4 0917+44	09 20 58.4584	+44 41 53.985	2.180	Q	18.2	178	15	5	Y
0919-260	PKS 0919-260	09 21 29.3538	–26 18 43.386	2.300	Q	18.4	285	8	10	...
0923+392	B2 0923+39	09 27 03.0139	+39 02 20.852	0.698	Q	17.0	88	15	8	...
0945+408	4C 40.24	09 48 55.3409	+40 39 44.583	1.252	Q	18.1	159	86	6	Y
0951+699[p]	MESSIER 082	09 55 52.725	+69 40 45.78	0.001	G	8.4	...	...	...	Y
0953+254	OK 290	09 56 49.8753	+25 15 16.050	0.712	Q	17.2	116	15	5	Y
0955+476	OK 492	09 58 19.6716	+47 25 07.842	1.873	Q	18.6	127	15	8	y
0954+658	S4 0954+65	09 58 47.2451	+65 33 54.818	0.367	B	16.8	289	86	6	Y
1034-293	PKS 1034-293	10 37 16.0797	–29 34 02.812	0.312	Q	16.5	34	5	3	...
1036+054[q]	PKS 1036+054	10 38 46.7798	+05 12 29.085	0.473	Q	19.5	351	15	8	...
1038+064	4C 06.41	10 41 17.1625	+06 10 16.924	1.265	Q	16.7	163	15	8	Y
1040+244	TEX 1040+244	10 43 09.0357	+24 08 35.409	0.560	B	17.7	88	8	10	Y

Table 1. continued.

Source name (IAU) (1)	Alias (2)	(J2000.0) (3)	(J2000.0) (4)	z (5)	Cl. (6)	V mag (7)	$\phi_{\rm jet}$ [°] (8)	$\nu_{\rm obs}$ [GHz] (9)	Ref. ($\phi_{\rm jet}$) (10)	*Fermi* 2LAC? (11)
1045-188	PKS 1045-18	10 48 06.6205	–19 09 35.726	0.595	Q	18.2	150	15	8	...
1044+719	S5 1044+71	10 48 27.6199	+71 43 35.938	1.150	Q	19.0	178	8	10	Y
1055+018	PKS 1055+01	10 58 29.6052	+01 33 58.824	0.888	Q	18.3	308	15	8	Y
1124-186	PKS 1124-186	11 27 04.3924	–18 57 17.440	1.048	Q	18.6	169	15	8	Y
1127-145	PKS 1127-14	11 30 07.0525	–14 49 27.387	1.187	Q	16.9	98	15	8	Y
1128+385	S4 1128+38	11 30 53.2826	+38 15 18.547	1.733	Q	19.5	203	86	6	...
1144+402	S4 1144+40	11 46 58.2979	+39 58 34.304	1.089	Q	18.0	5	8	10	Y
1150+497	LB 2136	11 53 24.4666	+49 31 08.830	0.334	Q	17.7	217	86	6	y
1150+812	S5 1150+81	11 53 12.4993	+80 58 29.154	1.250	Q	19.4	218	15	8	...
1155+169	PKS 1155+169	11 57 34.8362	+16 38 59.650	1.050	Q	18.2	...	...	...	...
1156+295	4C 29.45	11 59 31.8339	+29 14 43.827	0.729	Q	14.4	38	86	6	Y
1202-262	PKS 1203-26	12 05 33.2123	–26 34 04.464	0.786	Q	19.5	342	15	9	Y
1213-172[r]	PKS 1213-17	12 15 46.7517	-17 31 45.402	...	U	21.4	104	15	8	...
1216+061	NGC 4261	12 19 23.2204	+05 49 30.775	0.007	G	12.9	270	8	10	...
1226+023	3C 273	12 29 06.6997	+02 03 08.598	0.158	Q	12.8	208	15	8	Y
1228+126	NGC 4486	12 30 49.4233	+12 23 28.043	0.004	G	12.9	262	15	8	Y
1236+077	PKS 1236+077	12 39 24.5883	+07 30 17.189	0.400	G	19.2	317	24	10	Y
1244-255	PKS 1244-255	12 46 46.8020	–25 47 49.287	0.638	Q	17.4	138	15	9	Y
1253-055	3C 279	12 56 11.1665	–05 47 21.523	0.538	Q	17.8	215	15	8	Y
1308+326	B2 1308+32	13 10 28.6638	+32 20 43.783	0.997	Q	15.2	281	86	6	Y
1321-105	PKS 1321-105	13 24 25.7931	–10 49 23.133	0.872	Q	18.5	...	...	...	...
1324+224	B2 1324+22	13 27 00.8613	+22 10 50.163	1.400	Q	18.9	330	15	8	Y
1328+307	3C 286.0	13 31 08.2879	+30 30 32.958	0.846	Q	17.2	230	15	9	...
1330+022	3C 287.1	13 32 53.270	+02 00 45.70	0.216	G	18.5	245	5	3	...
1334-127	PKS 1335-127	13 37 39.7827	–12 57 24.692	0.539	Q	19.0	166	15	8	Y
1345+125	PKS 1345+12	13 47 33.3616	+12 17 24.240	0.121	G	18.5	164	15	5	...
1354-152	PKS 1354-152	13 57 11.2449	–15 27 28.785	1.890	Q	18.1	48	15	9	...
1354+195	PKS 1354+19	13 57 04.4366	+19 19 07.372	0.719	Q	16.0	146	15	9	...
1413+135	PKS 1413+135	14 15 58.8174	+13 20 23.713	0.247	B	20.5	247	15	8	Y
1417+385	B3 1417+385	14 19 46.6137	+38 21 48.475	1.832	Q	19.7	163	15	8	Y
1418+546	OQ 530	14 19 46.5974	+54 23 14.787	0.152	B	15.7	133	15	9	Y
1441+522	3C 303	14 43 02.759	+52 01 37.22	0.141	G	18.3	...	...	...	...
1502+106	PKS 1502+106	15 04 24.9797	+10 29 39.198	1.839	Q	18.6	131	86	6	Y
1504-166	PKS 1504-167	15 07 04.7869	–16 52 30.266	0.876	Q	18.5	205	15	8	...
1508-055	PKS 1508-05	15 10 53.5914	–05 43 07.417	1.191	Q	17.2	74	86	6	Y
1510-089	PKS 1510-089	15 12 50.5329	–09 05 59.828	0.360	Q	16.5	353	86	6	Y
1511-097[s]	WMAP J1513-0958	15 13 50.0	–09 58 29	...	U	...	...	...	...	...
1514-241	AP LIB	15 17 41.8131	–24 22 19.475	0.048	B	14.8	173	15	9	Y
1532+016	PKS 1532+01	15 34 52.4536	+01 31 04.206	1.420	Q	19.9	136	15	5	...
1546+027	PKS 1546+027	15 49 29.4368	+02 37 01.163	0.412	Q	17.4	183	86	6	Y
1548+056	PKS 1548+056	15 50 35.2692	+05 27 10.448	1.422	Q	19.5	1	86	6	Y
1606+105	PKS 1606+10	16 08 46.2031	+10 29 07.776	1.226	Q	18.7	307	15	5	Y
1611+343	DA 406	16 13 41.0642	+34 12 47.908	1.401	Q	18.1	164	15	8	Y
1622-297	PKS 1622-29	16 26 06.0208	–29 51 26.970	0.815	Q	19.5	252	43	2	Y
1633+382	B2 1633+38	16 35 15.4929	+38 08 04.500	1.807	Q	18.0	288	15	8	Y
1637+574	OS 562	16 38 13.4563	+57 20 23.978	0.751	Q	16.9	225	86	6	...
1641+399	3C 345	16 42 58.8099	+39 48 36.993	0.594	Q	16.6	275	15	8	y
1642+690[t]	4C 69.21	16 42 07.8485	+68 56 39.756	0.751	Q	20.5	164	15	5	...
1655+077	PKS 1655+077	16 58 09.0114	+07 41 27.540	0.621	Q	20.0	333	86	6	...
1726+455	S4 1726+45	17 27 27.6508	+45 30 39.731	0.714	Q	18.1	237	15	8	Y
1725+044	PKS 1725+044	17 28 24.9527	+04 27 04.913	0.293	Q	17.0	115	15	9	Y
1730-130	NRAO 530	17 33 02.7057	–13 04 49.547	0.902	Q	19.5	31	15	8	Y
1732+389	S4 1732+389	17 34 20.5785	+38 57 51.442	0.976	Q	20.6	89	5	3	Y
1738+476[u]	OT 465	17 39 57.1290	+47 37 58.361	0.954	B	17.5	274	5	11	Y
1739+522	4C +51.37	17 40 36.9778	+52 11 43.407	1.379	Q	18.7	41	86	6	Y
1741-038	PKS 1741-03	17 43 58.8561	–03 50 04.616	1.057	Q	20.4	237	86	6	...
1749+096[v]	OT 081	17 51 32.8185	+09 39 00.728	0.320	B	16.8	6	15	8	Y
1751+288[w]	B2 1751+28	17 53 42.4736	+28 48 04.938	1.118	Q	20.3	24	15	8	...
1803+784[x]	S5 1803+78	18 00 45.6839	+78 28 04.018	0.680	B	15.9	224	86	6	Y
1800+440	B3 1800+440	18 01 32.3149	+44 04 21.900	0.663	Q	17.9	271	86	6	Y
1807+698	3C 371	18 06 50.6806	+69 49 28.108	0.050	B	14.2	264	15	5	Y
1823+568[y]	4C 56.27	18 24 07.0683	+56 51 01.490	0.664	B	18.4	194	86	6	Y
1828+487	3C 380	18 29 31.7809	+48 44 46.160	0.692	Q	16.8	316	86	6	Y
1830-211	MC 1830-211	18 33 39.888	–21 03 39.77	2.507	Q	18.7	42	5	3	y

Table 1. continued.

Source name (IAU) (1)	Alias (2)	(J2000.0) (3)	(J2000.0) (4)	z (5)	Cl. (6)	V mag (7)	$\phi_{\rm jet}$ [°] (8)	$\nu_{\rm obs}$ [GHz] (9)	Ref. ($\phi_{\rm jet}$) (10)	*Fermi* 2LAC? (11)
1842+681	S4 1842+68	18 42 33.6416	+68 09 25.227	0.475	Q	18.1	117	86	6	...
1849+670	S4 1849+67	18 49 16.0723	+67 05 41.679	0.657	Q	16.9	324	15	8	Y
1908-201	TEX 1908-201	19 11 09.6528	–20 06 55.108	1.119	Q	18.1	4	15	9	Y
1920-211	TEX 1920-211	19 23 32.1898	–21 04 33.332	0.874	Q	17.5	342	15	9	Y
1921-293	OV-236	19 24 51.0559	–29 14 30.120	0.352	Q	18.2	335	86	6	Y
1923+210[e]	PKS B1923+210	19 25 59.6053	+21 06 26.161	...	U	16.1	245	86	6	...
1928+738	4C 73.18	19 27 48.4951	+73 58 01.569	0.303	Q	16.1	156	15	8	...
1957+405	CYGNUS A	19 59 28.3566	+40 44 02.096	0.056	G	15.1	283	15	8	...
1958-179	PKS 1958-179	20 00 57.0904	–17 48 57.672	0.652	Q	18.6	207	15	8	Y
2007+777	TEX 2005+403	20 05 30.9298	+77 52 43.137	0.342	B	16.7	282	86	6	...
2005+403	[HB89] 2005+403	20 07 44.9448	+40 29 48.604	1.736	Q	19.0	120	15	8	...
2008-159	PKS 2008-159	20 11 15.7109	–15 46 40.253	1.180	Q	18.3	8	15	8	...
2013+370[a]	TXS 2013+370	20 15 28.7298	+37 10 59.514	...	B	21.6	176	86	6	y
2021+614	OW 637	20 22 06.6817	+61 36 58.804	0.227	G	19.0	214	15	8	...
2023+336	B2 2023+33	20 25 10.8420	+33 43 00.214	0.219	B	...	344	86	6	y
2037+511	3C 418	20 38 37.0347	+51 19 12.662	1.687	Q	21.0	226	86	6	...
2059+034	PKS 2059+034	21 01 38.8341	+03 41 31.321	1.015	Q	17.8	30	8	10	...
2121+053	PKS 2121+053	21 23 44.5173	+05 35 22.093	1.941	Q	20.4	276	15	8	...
2127-096	PKS 2127-096	21 30 19.0882	–09 27 37.435	>0.780	Q	...	...	...	...	...
2128-123	PKS 2128-12	21 31 35.2617	–12 07 04.795	0.501	Q	16.1	216	15	8	...
2131-021[b]	PKS 2131-021	21 34 10.3096	–01 53 17.238	1.284	B	19.0	100	15	8	Y
2134+004	PKS 2134+004	21 36 38.5863	+00 41 54.213	1.932	Q	17.1	332	15	8	...
2136+141	PKS 2136+141	21 39 01.3092	+14 23 35.992	2.427	Q	18.9	310	15	8	...
2140-048	PKS 2140-048	21 42 36.9016	–04 37 43.512	0.344	Q	18.0	...	...	...	...
2145+067	PKS 2145+06	21 48 05.4586	+06 57 38.604	0.999	Q	16.5	122	15	8	Y
2155-152	PKS 2155-152	21 58 06.2819	–15 01 09.327	0.672	Q	18.3	207	15	8	Y
2200+420	BL LAC	22 02 43.2913	+42 16 39.979	0.069	B	14.7	221	86	6	Y
2201+171	PKS 2201+171	22 03 26.8936	+17 25 48.247	1.076	Q	19.5	37	15	8	Y
2201+315	B2 2201+31A	22 03 14.9757	+31 45 38.269	0.298	Q	15.6	209	15	8	...
2203-188	PKS 2203-18	22 06 10.4170	–18 35 38.746	0.619	Q	18.5	...	...	...	...
2209+236	PKS 2209+236	22 12 05.9663	+23 55 40.543	1.125	Q	20.7	32	15	8	Y
2216-038	PKS 2216-03	22 18 52.0377	–03 35 36.879	0.901	Q	16.4	188	15	8	...
2223-052	3C 446	22 25 47.2592	–04 57 01.390	1.404	Q	18.4	128	86	6	Y
2223+210	PKS 2223+21	22 25 38.0471	+21 18 06.414	1.953	Q	17.5	235	15	9	...
2227-088	PKS 2227-08	22 29 40.0843	–08 32 54.434	1.562	Q	17.4	312	15	8	Y
2230+114	CTA 102	22 32 36.4089	+11 43 50.904	1.037	Q	17.3	126	15	8	Y
2234+282	B2 2234+28A	22 36 22.4708	+28 28 57.413	0.795	Q	19.0	263	15	5	Y
2243-123	PKS 2243-123	22 46 18.2319	–12 06 51.277	0.630	Q	16.4	359	15	8	...
2251+158	3C 454.3	22 53 57.7479	+16 08 53.560	0.859	Q	16.1	255	86	6	Y
2255-282	PKS 2255-282	22 58 05.9628	–27 58 21.255	0.927	Q	16.8	224	15	9	Y
2325+093[c]	PKS 2325+093	23 27 33.5805	+09 40 09.462	1.843	Q	18.3	249	15	9	Y
2328+107	PKS 2328+10	23 30 40.8522	+11 00 18.710	1.489	Q	18.5	329	8	10	y
2342-161[d]	PMN J2345-1555	23 45 12.4623	–15 55 07.834	0.621	Q	18.4	316	15	9	Y
2345-167	PKS 2345-16	23 48 02.6085	–16 31 12.022	0.576	Q	18.4	121	86	6	Y
2346+385	S4 2346+38	23 49 20.8265	+38 49 17.558	1.032	Q	18.5	317	24	10	...
2353+816	S5 2353+81	23 56 22.82	+81 52 52.6	1.344	Q	20.3	340	15	9	...
2355-106	PKS 2355-106	23 58 10.8824	–10 20 08.610	1.622	Q	18.9	177	8	10	...

Table 2. Summary of observing results.

Source name (1)	MJD [d] (2)	t_{int} [min] (3)	S_{86} [Jy] (4)	$m_{86,L}$ [%] (5)	χ_{86} [°] (6)	$m_{86,C}$ [%] (7)	S_{229} [Jy] (8)	$m_{229,L}$ [%] (9)	χ_{229} [°] (10)	$\lvert RM^{upper\ limit}_{86,229}\rvert$ [rad m^{-2}] (11)
0003+380	55 422.9971	6.6	0.78 ± 0.04	4.6 ± 0.3	126.7 ± 2.3	<1.2	0.54 ± 0.03	<6.2	...	...
0003-066	55 406.0942	6.6	1.75 ± 0.09	11.6 ± 0.3	17.0 ± 0.7	<1.0	1.20 ± 0.06	16.7 ± 2.4	10.4 ± 4.0	2.04e+04
0007+106	55 423.0650	6.6	0.68 ± 0.03	3.1 ± 0.3	19.6 ± 3.1	<1.2	0.53 ± 0.03	<6.7	...	...
0017+200	55 423.1097	6.6	0.29 ± 0.01	4.1 ± 0.6	77.5 ± 3.6	<1.8	0.31 ± 0.02	<8.8	...	...
0027+056	55 423.0577	6.9	0.26 ± 0.01	5.1 ± 0.7	92.3 ± 3.9	<2.0	0.20 ± 0.01	<15.7	...	...
0035-252	55 423.1447	6.9	0.78 ± 0.04	1.4 ± 0.4	110.0 ± 6.9	<1.2	0.43 ± 0.03	<9.9	...	...
0045-255	55 423.1374	6.6	0.40 ± 0.02	<1.6	...	<1.7	0.79 ± 0.04	<7.5	...	...
0048-097	55 423.2353	6.6	0.17 ± 0.01	9.4 ± 1.0	88.4 ± 2.8	<3.2	0.14 ± 0.01	<19.9	...	...
0048-071	55 423.2452	6.6	0.74 ± 0.04	2.6 ± 0.3	72.5 ± 3.6	<1.1	0.33 ± 0.02	<9.7	...	...
0055+300	55 423.0269	6.6	0.51 ± 0.03	1.7 ± 0.4	159.8 ± 6.4	<1.3	0.26 ± 0.02	<11.1	...	...
0059+581	55 355.1482	3.3	2.12 ± 0.11	1.8 ± 0.2	48.5 ± 5.2	<1.0	1.36 ± 0.07	<5.3	...	...
0106+013	55 423.2751	3.3	2.44 ± 0.12	1.5 ± 0.3	174.8 ± 4.4	<1.0	1.52 ± 0.08	<5.2	...	...
0112-017	55 423.2650	6.6	0.22 ± 0.01	4.5 ± 0.7	82.6 ± 4.8	<2.6	0.42 ± 0.02	<7.1	...	...
0113-118	55 423.2552	6.6	1.24 ± 0.06	3.6 ± 0.3	23.4 ± 2.3	<1.1	0.36 ± 0.02	<9.3	...	...
0119+115	55 422.2371	6.6	0.92 ± 0.05	2.9 ± 0.4	168.2 ± 3.8	<1.4	0.37 ± 0.03	<20.1	...	...
0122-003	55 423.2830	6.6	0.47 ± 0.02	2.2 ± 0.5	6.4 ± 5.4	<1.5	0.12 ± 0.01	<26.1	...	...
0130-171	55 423.1206	3.4	1.89 ± 0.09	1.4 ± 0.3	18.4 ± 5.6	<1.1	0.74 ± 0.04	<9.3	...	...
0133+476	55 423.9159	6.6	1.63 ± 0.08	3.5 ± 0.2	137.7 ± 2.6	<1.0	0.13 ± 0.01	<30.8	...	...
0135-247	55 423.1276	6.6	1.42 ± 0.07	4.8 ± 0.2	51.4 ± 2.0	<1.0	0.80 ± 0.04	<7.4	...	...
0146+056	55 423.3139	6.6	0.29 ± 0.01	6.3 ± 0.6	110.8 ± 2.9	<1.9	<0.29	...	...	...
0149+218	55 422.2483	6.6	0.89 ± 0.04	<1.2	...	<1.4	0.23 ± 0.03	<30.6	...	...
0202+149	55 422.2202	3.4	0.71 ± 0.04	3.0 ± 0.5	131.5 ± 5.6	<1.8	0.36 ± 0.04	<27.1	...	...
0202+319	55 422.2673	2.4	1.04 ± 0.05	6.0 ± 0.5	89.5 ± 2.1	<1.7	0.16 ± 0.04	<72.4	...	...
0215+015	55 423.3239	6.9	1.21 ± 0.06	2.9 ± 0.3	113.3 ± 2.9	<1.0	0.60 ± 0.03	<9.2	...	...
0212+735	55 423.9487	6.6	1.23 ± 0.06	<1.0	...	<1.0	<1.23	...	...	...
0218+357	55 423.0165	6.6	0.70 ± 0.03	14.5 ± 0.3	47.0 ± 0.8	<1.2	0.57 ± 0.03	9.6 ± 2.3	42.7 ± 7.2	3.64e+04
0220+427	55 423.0381	6.6	0.14 ± 0.01	11.1 ± 1.2	142.5 ± 3.1	<3.6	<0.14	...	...	...
0224+671	55 423.9594	6.6	0.82 ± 0.04	5.2 ± 0.3	38.1 ± 2.0	<1.1	0.66 ± 0.03	<6.6	...	...
0229+131	55 423.3036	6.6	0.80 ± 0.04	2.1 ± 0.3	14.3 ± 4.1	−1.4 ± 0.4	<0.80	...	...	...
0234+285	55 423.2963	3.3	2.47 ± 0.12	<0.9	...	<1.0	1.73 ± 0.09	<4.8	...	...
0235+164	55 398.1411	3.3	1.46 ± 0.07	1.3 ± 0.3	18.9 ± 6.4	<1.1	0.96 ± 0.05	<5.7	...	...
0256-005	55 423.3349	6.6	0.32 ± 0.02	2.4 ± 0.6	24.9 ± 6.8	<1.9	0.20 ± 0.01	<14.5	...	...
0305+039	55 423.3447	6.6	0.38 ± 0.02	2.0 ± 0.5	166.8 ± 6.7	<1.6	0.11 ± 0.01	<28.5	...	...
0306+102	55 423.3547	6.9	1.21 ± 0.06	1.9 ± 0.3	27.1 ± 4.5	<1.0	0.83 ± 0.04	<5.6	...	...
0316+413	55 355.2039	1.7	12.84 ± 0.64	0.8 ± 0.2	31.4 ± 10.8	<1.0	6.19 ± 0.31	5.3 ± 1.6	20.3 ± 8.5	6.94e+04
0327-241	55 424.2121	6.9	0.56 ± 0.03	6.3 ± 0.4	117.9 ± 2.0	<1.4	0.22 ± 0.02	<16.4	...	...
0336-019	55 406.2183	6.6	2.12 ± 0.11	1.7 ± 0.3	88.0 ± 3.9	<1.0	1.42 ± 0.08	<6.6	...	...
0338-214	55 424.1931	6.6	0.47 ± 0.02	<1.5	...	<1.5	0.29 ± 0.02	<12.2	...	...
0346-163	55 423.3749	6.8	0.71 ± 0.04	5.4 ± 0.4	103.8 ± 1.7	<1.3	0.57 ± 0.03	10.1 ± 2.8	97.6 ± 8.0	4.14e+04
0356+102	55 423.3645	6.6	<0.10	...	...	...	<0.10	...	...	...
0355+508	55 406.1763	3.3	6.61 ± 0.33	1.8 ± 0.2	145.9 ± 4.7	<1.0	3.48 ± 0.18	<5.1	...	...
0403-132	55 423.3848	6.6	0.53 ± 0.03	6.7 ± 0.4	173.9 ± 1.6	<1.3	<0.53	...	...	...

Notes. Columns are as follows: (1) IAU B1950.0 source name; (2) MJD observing date; (3) integration time; (4) 86.2 GHz flux density; (5) 86.2 GHz fractional linear polarization; (6) 86.2 GHz linear polarization electric vector position angle; (7) 86.2 GHz fractional circular polarization; (8) 229 GHz flux density; (9) 229 GHz fractional linear polarization; (10) 229 GHz linear polarization electric vector position angle; (11) Absolute value of the maximum rotation measure allowed from χ_{86} and χ_{229}, and computed as a 3σ value.

Table 2. continued.

Source name (1)	MJD [d] (2)	$t_{\rm int}$ [min] (3)	S_{86} [Jy] (4)	$m_{86,\rm L}$ [%] (5)	χ_{86} [°] (6)	$m_{86,\rm C}$ [%] (7)	S_{229} [Jy] (8)	$m_{229,\rm L}$ [%] (9)	χ_{229} [°] (10)	$\lvert {\rm RM}^{\rm upper\,limit}_{86,229}\rvert$ [rad m^{-2}] (11)
0415+379	55 398.1589	3.3	2.58 ± 0.13	<0.9	...	<1.0	1.29 ± 0.07	<5.4	...	...
0420-014	55 424.2226	3.3	4.77 ± 0.24	2.1 ± 0.3	9.0 ± 2.9	<1.0	2.77 ± 0.14	5.5 ± 1.6	12.7 ± 8.1	4.36e+04
0422+004	55 422.3899	6.6	0.25 ± 0.01	5.1 ± 0.8	27.4 ± 4.5	<2.5	0.12 ± 0.02	<36.3	...	...
0430+052	55 422.3767	6.6	0.86 ± 0.04	2.4 ± 0.3	170.3 ± 3.6	−1.5 ± 0.4	<0.86	...	...	...
0440-003	55 544.8442	6.6	0.65 ± 0.03	6.0 ± 0.3	19.7 ± 1.6	<1.2	0.35 ± 0.02	<7.3	...	...
0451-282	55 424.3113	3.3	1.97 ± 0.10	1.6 ± 0.3	179.2 ± 4.3	−1.1 ± 0.4	0.45 ± 0.03	<12.0	...	...
0454-234	55 424.3014	6.6	1.31 ± 0.07	2.0 ± 0.3	5.3 ± 3.5	<1.0	0.73 ± 0.04	7.9 ± 2.0	164.9 ± 7.3	4.10e+04
0458-020	55 423.4484	6.6	1.17 ± 0.06	5.0 ± 0.3	111.4 ± 1.7	<1.1	0.81 ± 0.04	<6.8	...	...
0516-054	55 424.1811	6.6	<0.10	...	...	...	0.13 ± 0.01	<29.0	...	...
0528+134	55 423.4261	3.3	0.96 ± 0.05	1.7 ± 0.3	132.9 ± 6.5	<1.2	0.37 ± 0.02	<11.0	...	...
0529+075	55 423.4383	6.6	1.27 ± 0.06	2.4 ± 0.3	150.7 ± 3.6	<1.0	0.86 ± 0.04	<5.6	...	...
0548+378	55 424.1625	6.6	0.12 ± 0.01	<4.6	...	<4.2	0.12 ± 0.01	<24.6	...	...
0552+398	55 424.1554	6.9	1.46 ± 0.07	1.6 ± 0.3	122.4 ± 5.6	<1.0	0.68 ± 0.04	<6.0	...	...
0605-085	55 423.4712	6.6	1.60 ± 0.08	2.5 ± 0.3	110.6 ± 3.2	<1.0	0.59 ± 0.03	<8.2	...	...
0607-157	55 423.4612	6.6	1.46 ± 0.07	1.7 ± 0.2	46.3 ± 5.6	<1.0	0.26 ± 0.02	<22.7	...	...
0627-199	55 423.4017	6.6	0.96 ± 0.05	6.2 ± 0.3	66.8 ± 1.5	<1.1	0.27 ± 0.02	<12.9	...	...
0631-223	55 728.5979	6.6	0.30 ± 0.02	<2.2	...	<2.3	0.11 ± 0.02	<50.4	...	...
0642+449	55 424.2618	6.6	1.84 ± 0.09	4.4 ± 0.2	149.3 ± 1.9	<1.0	0.89 ± 0.05	6.4 ± 1.7	137.1 ± 7.6	3.96e+04
0646-176	55 434.4838	6.9	0.31 ± 0.02	9.8 ± 0.9	99.3 ± 2.6	<2.7	<0.31	...	...	...
0650+273	55 728.5906	6.8	<0.10	...	...	...	<0.10	...	...	...
0716+714	55 355.2478	3.3	2.16 ± 0.11	2.6 ± 0.3	83.1 ± 2.7	−1.3 ± 0.3	1.25 ± 0.07	<6.8	...	...
0723-008	55 424.3314	3.3	3.34 ± 0.17	3.7 ± 0.3	15.9 ± 1.9	<1.0	2.30 ± 0.12	<4.8	...	...
0727-115	55 423.4865	6.6	3.38 ± 0.17	7.6 ± 0.2	50.1 ± 1.2	<1.0	0.53 ± 0.03	<8.4	...	...
0730+504	55 424.2514	6.6	0.66 ± 0.03	<1.1	...	<1.2	0.29 ± 0.02	<10.9	...	...
0735+178	55 434.5187	6.9	0.46 ± 0.02	2.7 ± 0.5	162.8 ± 5.1	<1.6	0.19 ± 0.02	<30.7	...	...
0736+017	55 424.3386	6.6	0.98 ± 0.05	2.2 ± 0.3	97.8 ± 3.5	<1.1	0.80 ± 0.04	<8.4	...	...
0738+313	55 434.5557	6.6	0.44 ± 0.02	4.3 ± 0.5	82.7 ± 3.2	<1.6	<0.44	...	...	...
0745+241	55 434.5630	6.6	1.02 ± 0.05	9.1 ± 0.3	77.6 ± 0.9	<1.1	0.24 ± 0.02	<28.5	...	...
0748+126	55 434.5259	6.6	2.37 ± 0.12	3.4 ± 0.3	28.6 ± 2.4	<1.0	0.98 ± 0.05	<7.1	...	...
0754+100	55 434.5331	6.6	1.00 ± 0.05	4.4 ± 0.3	166.6 ± 1.9	<1.1	0.50 ± 0.03	<14.5	...	...
0805-077	55 423.4991	6.6	1.47 ± 0.07	5.6 ± 0.3	168.5 ± 1.3	<1.0	0.42 ± 0.02	<10.5	...	...
0814+425	55 357.8540	6.6	0.97 ± 0.05	7.4 ± 0.3	160.7 ± 1.2	<1.1	0.36 ± 0.02	<8.4	...	...
0820+225	55 422.6078	6.6	0.43 ± 0.02	1.9 ± 0.5	172.9 ± 7.9	<1.5	0.19 ± 0.01	<17.6	...	...
0821+394	55 424.2723	6.6	0.58 ± 0.03	5.0 ± 0.3	48.7 ± 2.3	<1.3	0.32 ± 0.02	<9.6	...	...
0823+033	55 424.4798	6.6	0.81 ± 0.04	<1.0	...	<2.2	0.34 ± 0.02	<8.3	...	...
0823-223	55 434.4915	6.9	0.51 ± 0.03	<1.6	...	<1.6	0.30 ± 0.03	<31.9	...	...
0827+243	55 434.5441	3.3	2.83 ± 0.14	2.8 ± 0.2	44.4 ± 3.2	<1.0	1.30 ± 0.07	<6.9	...	...
0834-201	55 423.5275	6.6	0.63 ± 0.03	<1.1	...	<1.3	0.40 ± 0.02	<13.1	...	...
0838+133	55 434.5775	6.6	0.88 ± 0.04	2.1 ± 0.3	148.0 ± 5.2	<1.2	<0.88	...	...	...
0836+710	55 406.1951	6.6	2.39 ± 0.12	<0.8	...	<1.0	0.58 ± 0.05	<18.8	...	...
0845-068	55 423.4141	6.6	0.49 ± 0.02	2.7 ± 0.4	102.5 ± 4.1	<1.4	0.19 ± 0.01	<18.6	...	...
0851+202	55 434.5733	3.3	2.44 ± 0.12	4.2 ± 0.3	150.2 ± 2.1	<1.0	0.50 ± 0.04	<16.3	...	...
0859-140	55 424.4983	6.6	0.22 ± 0.01	8.4 ± 0.9	139.7 ± 2.9	<2.5	<0.22	...	...	...
0906+015	55 424.5195	3.3	2.73 ± 0.14	<0.9	...	<2.2	0.26 ± 0.02	<20.5	...	...
0912+029	55 424.5441	6.6	0.60 ± 0.03	3.8 ± 0.4	150.4 ± 3.1	<1.2	0.22 ± 0.01	<15.9	...	...
0915-118	55 424.5091	6.6	0.40 ± 0.02	7.8 ± 0.5	117.2 ± 1.9	<1.6	0.33 ± 0.02	<11.8	...	...

Table 2. continued.

Source name (1)	MJD [d] (2)	$t_{\rm int}$ [min] (3)	S_{86} [Jy] (4)	$m_{86,\rm L}$ [%] (5)	χ_{86} [°] (6)	$m_{86,\rm C}$ [%] (7)	S_{229} [Jy] (8)	$m_{229,\rm L}$ [%] (9)	χ_{229} [°] (10)	$\lvert {\rm RM}^{\rm upper\,limit}_{86,229}\rvert$ [rad m^{-2}] (11)
0917+449	55 422.6490	6.6	1.49 ± 0.07	1.6 ± 0.2	140.1 ± 5.9	1.5 ± 0.3	0.46 ± 0.03	<9.6	...	...
0919-260	55 423.5412	6.6	0.58 ± 0.03	3.5 ± 0.5	177.6 ± 3.3	<1.5	<0.58	...	...	...
0923+392	55 422.6276	3.3	4.88 ± 0.24	3.4 ± 0.2	146.9 ± 2.5	–2.1 ± 0.3	1.46 ± 0.07	<8.4	...	...
0945+408	55 422.6388	6.6	0.52 ± 0.03	4.4 ± 0.4	98.5 ± 2.5	<1.3	<0.52	...	...	...
0951+699	55 423.7417	6.6	0.44 ± 0.02	2.8 ± 0.5	48.9 ± 5.6	<1.6	<0.44	...	...	...
0953+254	55 434.5879	6.6	1.02 ± 0.05	4.3 ± 0.3	71.7 ± 2.0	<1.1	<1.02	...	...	...
0955+476	55 422.6596	6.6	0.46 ± 0.02	6.4 ± 0.5	34.9 ± 2.3	<1.5	0.86 ± 0.05	<6.7	...	...
0954+658	55 379.4743	6.6	1.14 ± 0.06	11.2 ± 0.3	174.8 ± 0.7	–1.2 ± 0.4	0.18 ± 0.02	<37.7	...	...
1034-293	55 423.5655	6.6	1.54 ± 0.08	3.6 ± 0.3	170.1 ± 2.0	<1.1	0.23 ± 0.02	<25.6	...	...
1036+054	55 424.5559	6.6	0.53 ± 0.03	1.4 ± 0.4	25.6 ± 8.1	<1.3	0.39 ± 0.02	<9.2	...	...
1038+064	55 357.8273	6.6	1.14 ± 0.06	1.6 ± 0.3	94.6 ± 4.3	<1.0	0.27 ± 0.02	<10.6	...	...
1040+244	55 424.7770	6.6	0.74 ± 0.04	4.8 ± 0.6	82.8 ± 3.3	<1.7	<0.74	...	...	...
1045-188	55 423.5763	6.6	0.91 ± 0.05	1.9 ± 0.4	79.5 ± 4.4	<1.1	<0.91	...	...	...
1044+719	55 423.7345	6.6	0.56 ± 0.03	2.1 ± 0.4	54.4 ± 6.4	<1.4	<0.56	...	...	...
1055+018	55 452.5101	3.3	3.97 ± 0.20	7.7 ± 0.2	135.9 ± 1.1	<1.0	1.55 ± 0.08	10.8 ± 2.2	143.9 ± 5.7	2.94e+04
1124-186	55 423.5871	6.6	1.32 ± 0.07	3.1 ± 0.3	176.1 ± 2.4	–2.0 ± 0.3	0.49 ± 0.03	<11.8	...	...
1127-145	55 434.6131	6.9	1.79 ± 0.09	1.6 ± 0.3	159.5 ± 5.0	<1.0	0.30 ± 0.03	<33.4	...	...
1128+385	55 423.7059	6.6	0.66 ± 0.03	3.8 ± 0.4	169.5 ± 2.5	<1.3	0.18 ± 0.02	<23.3	...	...
1144+402	55 423.6954	6.6	0.76 ± 0.04	5.8 ± 0.4	88.3 ± 1.5	<1.2	0.59 ± 0.03	<8.7	...	...
1150+497	55 423.6832	6.6	1.69 ± 0.08	3.6 ± 0.2	50.0 ± 2.5	<1.0	0.17 ± 0.02	<25.4	...	...
1150+812	55 423.7522	6.6	0.37 ± 0.02	4.3 ± 0.6	160.5 ± 3.7	<1.8	0.49 ± 0.03	<10.3	...	...
1155+169	55 424.5668	6.9	0.30 ± 0.02	7.8 ± 0.5	167.0 ± 1.9	<1.8	0.23 ± 0.02	<11.1	...	...
1156+295	55 321.9940	6.6	2.25 ± 0.11	2.0 ± 0.3	158.0 ± 3.8	<1.0	1.63 ± 0.08	<4.6	...	...
1202-262	55 434.6206	6.6	0.41 ± 0.02	<2.2	...	<2.2	0.18 ± 0.04	<78.9	...	...
1213-172	55 423.5979	6.6	0.78 ± 0.04	5.0 ± 0.4	74.1 ± 1.9	<1.2	0.74 ± 0.04	<8.2	...	...
1216+061	55 424.5794	6.6	0.32 ± 0.02	<1.9	...	<1.9	<0.32	...	...	...
1226+023	55 434.4696	1.7	15.37 ± 0.77	3.4 ± 0.2	151.1 ± 2.4	<1.0	6.79 ± 0.34	<4.8	...	...
1228+126	55 357.8105	3.3	4.46 ± 0.22	4.2 ± 0.2	40.5 ± 2.1	<1.0	1.51 ± 0.08	<4.9	...	...
1236+077	55 424.5897	6.6	0.66 ± 0.03	6.0 ± 0.4	97.7 ± 1.6	<1.3	0.28 ± 0.02	<13.7	...	...
1244-255	55 423.6191	6.6	1.05 ± 0.05	2.0 ± 0.3	144.7 ± 5.4	<1.2	<1.05	...	...	...
1253-055	55 434.6438	1.7	14.34 ± 0.72	3.9 ± 0.3	107.8 ± 1.8	<1.0	6.05 ± 0.31	<6.6	...	...
1308+326	55 322.0148	6.6	2.40 ± 0.12	2.7 ± 0.3	106.8 ± 2.6	<1.0	1.53 ± 0.08	<4.6	...	...
1321-105	55 424.8005	6.6	0.31 ± 0.02	5.0 ± 1.0	112.6 ± 5.7	<3.4	<0.31	...	...	...
1324+224	55 501.4942	6.6	0.72 ± 0.04	1.4 ± 0.4	166.1 ± 6.3	–1.3 ± 0.4	0.46 ± 0.02	<7.1	...	...
1328+307	55 593.1857	6.6	0.87 ± 0.04	13.4 ± 0.3	33.0 ± 0.7	–1.1 ± 0.4	0.31 ± 0.02	<7.3	...	...
1330+022	55 434.6491	6.6	0.54 ± 0.03	1.8 ± 0.4	129.2 ± 7.2	<1.5	0.36 ± 0.03	<16.0	...	...
1334-127	55 423.6375	3.3	2.45 ± 0.12	6.1 ± 0.3	15.9 ± 1.2	<1.0	0.95 ± 0.06	<10.8	...	...
1345+125	55 452.6632	3.3	0.51 ± 0.03	<1.6	...	<1.9	0.35 ± 0.03	<22.4	...	...
1354-152	55 434.6567	6.6	0.35 ± 0.02	2.6 ± 0.7	62.0 ± 7.5	<2.1	0.13 ± 0.03	<59.8	...	...
1354+195	55 501.5185	6.6	0.92 ± 0.05	1.0 ± 0.3	74.6 ± 8.3	<1.1	<0.92	...	...	...
1413+135	55 501.5291	6.6	0.35 ± 0.02	<1.5	...	<1.6	<0.35	...	...	...
1417+385	55 593.1945	6.6	0.31 ± 0.02	3.1 ± 0.5	177.7 ± 4.4	<1.5	0.12 ± 0.01	<14.1	...	...
1418+546	55 423.9711	6.6	0.65 ± 0.03	3.0 ± 0.4	119.0 ± 4.0	<1.3	<0.65	...	...	...
1441+522	55 423.9811	6.6	0.51 ± 0.03	2.2 ± 0.4	133.2 ± 5.9	<1.4	0.32 ± 0.02	<12.2	...	...
1502+106	55 501.5399	6.6	0.70 ± 0.04	3.9 ± 0.3	128.3 ± 2.7	<1.2	0.46 ± 0.02	<6.7	...	...

Table 2. continued.

Source name (1)	MJD [d] (2)	$t_{\rm int}$ [min] (3)	S_{86} [Jy] (4)	$m_{86,\rm L}$ [%] (5)	χ_{86} [°] (6)	$m_{86,\rm C}$ [%] (7)	S_{229} [Jy] (8)	$m_{229,\rm L}$ [%] (9)	χ_{229} [°] (10)	$\lvert {\rm RM}^{\rm upper\,limit}_{86,229}\rvert$ [rad m^{-2}] (11)
1504-166	55 424.8325	6.9	0.50 ± 0.03	6.0 ± 0.6	90.6 ± 2.6	<2.1	0.27 ± 0.05	<56.3	...	...
1508-055	55 424.8472	6.6	0.68 ± 0.03	8.6 ± 0.5	79.5 ± 1.4	<1.4	0.52 ± 0.06	<27.2	...	...
1510-089	55 424.8222	6.6	1.75 ± 0.09	2.6 ± 0.3	106.1 ± 2.9	<1.1	1.02 ± 0.06	<9.5	...	...
1511-097	55 593.2064	6.6	<0.10	...	...	...	<0.10	...	...	...
1514-241	55 434.6671	6.6	1.89 ± 0.09	1.5 ± 0.3	5.8 ± 4.7	<1.0	0.75 ± 0.05	<15.2	...	...
1532+016	55 422.8835	6.6	0.57 ± 0.03	2.5 ± 0.4	86.0 ± 4.4	<1.3	<0.57	...	...	...
1546+027	55 422.8733	6.6	1.42 ± 0.07	3.5 ± 0.2	46.8 ± 2.7	<1.0	0.74 ± 0.04	<6.3	...	...
1548+056	55 422.8558	6.6	1.71 ± 0.09	2.0 ± 0.3	151.3 ± 4.4	<1.0	0.79 ± 0.04	8.8 ± 2.4	162.2 ± 7.4	4.33e+04
1606+105	55 422.8631	6.6	0.43 ± 0.02	<1.4	...	<1.4	0.23 ± 0.02	<17.5	...	...
1611+343	55 398.1037	6.6	1.34 ± 0.07	4.4 ± 0.3	12.2 ± 1.8	<1.1	0.45 ± 0.03	<9.3	...	...
1622-297	55 322.0714	6.6	2.12 ± 0.11	3.2 ± 0.3	83.1 ± 2.0	<1.0	0.95 ± 0.05	<5.0	...	...
1633+382	55 398.1145	3.3	3.44 ± 0.17	2.1 ± 0.2	119.2 ± 4.0	<1.0	1.79 ± 0.09	<5.2	...	...
1637+574	55 423.8010	6.6	0.94 ± 0.05	2.9 ± 0.3	169.6 ± 2.7	<1.1	0.64 ± 0.03	<6.1	...	...
1641+399	55 422.9297	3.3	5.25 ± 0.26	5.3 ± 0.3	74.6 ± 1.3	<1.0	2.56 ± 0.13	7.1 ± 1.7	89.3 ± 7.0	3.60e+04
1642+690	55 423.8113	6.6	0.97 ± 0.05	1.1 ± 0.3	144.6 ± 9.0	−1.3 ± 0.4	0.47 ± 0.03	<7.7	...	...
1655+077	55 423.9922	6.6	1.41 ± 0.07	9.1 ± 0.3	124.1 ± 1.0	<1.1	0.91 ± 0.05	7.2 ± 2.1	124.5 ± 8.3	4.19e+04
1726+455	55 422.9369	6.6	1.05 ± 0.05	3.3 ± 0.2	131.6 ± 2.9	<1.0	0.89 ± 0.05	<5.8	...	...
1725+044	55 423.9996	6.6	1.26 ± 0.06	<0.7	...	<1.1	0.76 ± 0.04	<7.1	...	...
1730-130	55 398.0436	3.3	4.00 ± 0.20	2.7 ± 0.2	48.0 ± 3.3	<1.0	1.59 ± 0.08	<5.6	...	...
1732+389	55 422.9067	6.6	0.96 ± 0.05	1.8 ± 0.3	110.6 ± 4.8	<1.1	0.56 ± 0.03	<8.3	...	...
1738+476	55 422.9470	6.6	0.40 ± 0.02	4.1 ± 0.4	54.3 ± 3.3	<1.5	0.19 ± 0.01	<13.8	...	...
1739+522	55 423.8217	7.1	0.70 ± 0.03	5.3 ± 0.4	2.5 ± 1.5	<1.2	0.39 ± 0.02	<8.7	...	...
1741-038	55 424.0069	6.9	2.19 ± 0.11	1.4 ± 0.3	151.6 ± 5.8	<1.0	0.89 ± 0.05	<7.0	...	...
1749+096	55 434.7023	6.6	2.33 ± 0.12	3.4 ± 0.3	23.8 ± 2.3	<1.0	1.04 ± 0.05	<8.3	...	...
1751+288	55 422.8957	6.6	0.31 ± 0.02	6.5 ± 0.6	152.3 ± 2.8	<1.8	0.12 ± 0.02	<31.1	...	...
1803+784	55 423.7802	6.6	2.01 ± 0.10	9.3 ± 0.3	104.7 ± 0.8	<1.0	0.92 ± 0.05	8.1 ± 2.0	103.9 ± 7.1	3.61e+04
1800+440	55 422.9169	6.6	0.65 ± 0.03	1.2 ± 0.4	82.1 ± 8.3	<1.2	0.29 ± 0.02	<17.5	...	...
1807+698	55 355.1276	6.9	1.14 ± 0.06	2.4 ± 0.2	46.8 ± 3.9	<1.0	0.90 ± 0.05	6.5 ± 1.8	60.3 ± 8.1	4.54e+04
1823+568	55 355.1166	6.6	1.30 ± 0.06	12.0 ± 0.3	16.6 ± 0.6	<1.0	0.83 ± 0.04	16.2 ± 2.9	28.9 ± 5.0	2.57e+04
1828+487	55 422.9570	6.6	2.20 ± 0.11	3.7 ± 0.2	127.2 ± 2.3	<1.0	1.19 ± 0.06	<4.9	...	...
1830-211	55 422.9752	3.4	2.66 ± 0.13	2.1 ± 0.2	46.6 ± 4.3	<1.0	1.23 ± 0.06	<6.3	...	...
1842+681	55 423.8324	6.9	0.49 ± 0.02	3.7 ± 0.4	67.9 ± 3.5	<1.4	0.32 ± 0.02	<12.0	...	...
1849+670	55 423.8395	6.6	2.13 ± 0.11	3.6 ± 0.3	22.7 ± 2.2	<1.0	0.96 ± 0.05	7.3 ± 2.1	16.6 ± 8.0	4.17e+04
1908-201	55 424.0176	6.6	1.91 ± 0.10	<0.8	...	<1.0	0.76 ± 0.04	<7.6	...	...
1920-211	55 424.0249	6.6	1.93 ± 0.10	2.3 ± 0.2	55.9 ± 3.8	<1.0	0.91 ± 0.05	<6.8	...	...
1921-293	55 422.9696	1.7	11.24 ± 0.56	9.5 ± 0.3	107.5 ± 0.7	<1.0	6.23 ± 0.31	7.8 ± 1.6	107.3 ± 5.7	2.92e+04
1923+210	55 424.0356	6.6	1.05 ± 0.05	1.9 ± 0.3	155.6 ± 4.5	<1.1	0.46 ± 0.02	<6.7	...	...
1928+738	55 423.7906	6.6	3.07 ± 0.15	2.8 ± 0.3	98.3 ± 2.2	<1.0	1.88 ± 0.09	<4.8	...	...
1957+405	55 406.1173	6.6	1.28 ± 0.06	<0.8	...	<1.1	0.88 ± 0.05	7.7 ± 2.5	48.2 ± 9.6	...
1958-179	55 423.0768	6.6	1.42 ± 0.07	4.8 ± 0.3	114.1 ± 1.8	<1.1	0.64 ± 0.04	<10.6	...	...
2007+777	55 423.7653	6.6	0.51 ± 0.03	5.6 ± 0.4	113.4 ± 2.3	<1.4	<0.51	...	...	...
2005+403	55 423.8790	6.6	1.90 ± 0.10	3.5 ± 0.2	135.1 ± 2.5	<1.0	0.40 ± 0.02	<8.5	...	...
2008-159	55 423.0841	6.6	1.01 ± 0.05	1.6 ± 0.3	35.0 ± 6.6	<1.2	0.90 ± 0.05	<10.5	...	...
2013+370	55 423.8964	6.6	3.92 ± 0.20	1.2 ± 0.3	78.3 ± 5.5	<1.0	2.43 ± 0.12	<4.6	...	...
2021+614	55 423.8500	6.6	0.37 ± 0.02	<1.8	...	<1.9	<0.37	...	...	...

Table 2. continued.

Source name (1)	MJD [d] (2)	$t_{\rm int}$ [min] (3)	S_{86} [Jy] (4)	$m_{86,\rm L}$ [%] (5)	χ_{86} [°] (6)	$m_{86,\rm C}$ [%] (7)	S_{229} [Jy] (8)	$m_{229,\rm L}$ [%] (9)	χ_{229} [°] (10)	$\lvert \mathrm{RM}^{\rm upper\,limit}_{86,229} \rvert$ [rad m^{-2}] (11)
2023+336	55 423.9039	6.6	2.92 ± 0.15	4.6 ± 0.2	61.9 ± 1.7	<1.0	1.72 ± 0.09	<4.6	...	...
2037+511	55 423.8601	6.6	1.61 ± 0.08	2.2 ± 0.3	70.9 ± 3.5	<1.0	0.55 ± 0.03	<8.3	...	...
2059+034	55 423.1741	6.6	0.85 ± 0.04	2.8 ± 0.4	118.7 ± 4.0	<1.2	0.28 ± 0.03	<25.9	...	...
2121+053	55 424.1343	6.6	0.98 ± 0.05	4.2 ± 0.3	35.1 ± 2.3	<1.1	0.63 ± 0.03	<6.2	...	...
2127-096	55 424.0930	6.6	0.42 ± 0.02	7.1 ± 0.5	37.7 ± 2.0	<1.6	0.19 ± 0.01	<16.6	...	...
2128-123	55 424.0857	6.6	0.99 ± 0.05	1.8 ± 0.3	60.7 ± 5.2	<1.1	0.30 ± 0.02	<10.6	...	...
2131-021	55 423.1856	6.6	1.61 ± 0.08	9.0 ± 0.3	73.6 ± 0.9	−1.4 ± 0.3	0.38 ± 0.03	<18.0	...	...
2134+004	55 424.1031	6.6	2.18 ± 0.11	4.0 ± 0.3	172.6 ± 1.6	<1.0	0.88 ± 0.04	7.7 ± 1.8	172.0 ± 6.6	3.41e+04
2136+141	55 424.1196	6.6	0.98 ± 0.05	2.0 ± 0.3	130.4 ± 4.8	<1.1	0.38 ± 0.02	<7.7	...	...
2140-048	55 424.0732	6.6	0.17 ± 0.01	11.0 ± 1.0	68.6 ± 2.5	<3.2	0.33 ± 0.02	<9.2	...	...
2145+067	55 424.1301	3.5	2.54 ± 0.13	2.1 ± 0.2	53.7 ± 4.2	<1.0	1.24 ± 0.06	<5.6	...	...
2155-152	55 398.0904	6.6	1.81 ± 0.09	9.0 ± 0.3	19.2 ± 0.8	<1.0	0.61 ± 0.03	9.6 ± 2.1	22.2 ± 6.1	3.12e+04
2200+420	55 398.1305	3.3	6.35 ± 0.32	12.1 ± 0.3	21.6 ± 0.6	<1.0	5.48 ± 0.27	12.0 ± 1.5	18.6 ± 3.6	1.85e+04
2201+171	55 422.1068	6.9	1.22 ± 0.06	1.2 ± 0.3	145.4 ± 7.6	<1.1	0.74 ± 0.04	<10.3	...	...
2201+315	55 398.0792	6.8	2.19 ± 0.11	1.9 ± 0.2	142.0 ± 4.5	<1.0	1.19 ± 0.06	<4.7	...	...
2203-188	55 423.1556	6.6	0.65 ± 0.03	5.0 ± 0.4	37.5 ± 2.6	<1.4	<0.65	...	...	...
2209+236	55 422.0855	6.6	0.41 ± 0.02	5.5 ± 0.5	55.4 ± 2.6	<1.6	0.31 ± 0.03	<16.9	...	...
2216-038	55 424.0658	6.6	0.85 ± 0.04	1.3 ± 0.3	148.8 ± 7.8	<1.1	0.49 ± 0.03	<7.0	...	...
2223-052	55 398.0333	3.3	3.65 ± 0.18	1.0 ± 0.3	102.8 ± 6.8	<1.0	1.55 ± 0.08	<5.0	...	...
2223+210	55 422.0741	6.6	1.07 ± 0.05	2.7 ± 0.3	128.2 ± 3.6	<1.1	0.24 ± 0.02	<21.9	...	...
2227-088	55 424.0589	3.3	2.37 ± 0.12	1.9 ± 0.2	39.8 ± 4.7	<1.0	1.79 ± 0.09	5.5 ± 1.7	37.7 ± 8.5	4.92e+04
2230+114	55 398.0230	6.6	2.08 ± 0.10	3.6 ± 0.3	65.1 ± 2.2	<1.0	0.99 ± 0.05	6.1 ± 1.6	57.6 ± 7.7	4.04e+04
2234+282	55 422.0964	6.6	1.45 ± 0.07	3.4 ± 0.3	72.0 ± 2.3	<1.0	1.02 ± 0.06	<7.3	...	...
2243-123	55 423.1968	6.6	1.06 ± 0.05	4.4 ± 0.4	85.8 ± 1.8	<1.1	0.24 ± 0.02	<24.3	...	...
2251+158	55 423.1059	1.7	34.18 ± 1.71	1.5 ± 0.2	118.2 ± 5.1	<1.0	26.37 ± 1.32	<4.5	...	...
2255-282	55 423.0952	3.3	2.62 ± 0.13	1.3 ± 0.3	11.0 ± 5.6	<1.0	1.03 ± 0.06	<9.2	...	...
2325+093	55 422.0616	6.9	1.02 ± 0.05	2.3 ± 0.3	172.9 ± 3.4	<1.1	0.54 ± 0.03	<8.5	...	...
2328+107	55 422.0509	6.6	0.43 ± 0.02	3.3 ± 0.5	102.5 ± 4.0	<1.5	0.38 ± 0.02	<13.2	...	...
2342-161	55 423.2078	6.8	0.60 ± 0.03	4.3 ± 0.5	89.1 ± 2.5	−1.4 ± 0.4	0.28 ± 0.02	<14.7	...	...
2345-167	55 355.2684	3.3	1.65 ± 0.08	4.8 ± 0.2	48.2 ± 2.0	<1.0	1.10 ± 0.06	7.7 ± 2.0	68.9 ± 7.6	3.96e+04
2346+385	55 423.0043	6.6	0.32 ± 0.02	3.0 ± 0.5	7.2 ± 4.4	<1.7	0.27 ± 0.02	<7.8	...	...
2353+816	55 423.9413	6.9	0.49 ± 0.02	4.5 ± 0.4	35.9 ± 2.8	<1.4	0.44 ± 0.02	<7.1	...	...
2355-106	55 423.2244	6.6	0.52 ± 0.03	<1.4	...	<1.4	0.22 ± 0.02	<17.7	...	...